



HAL
open science

Effects of salts on the exchanges through high-pressure ice layers of large ocean worlds

Laëtitia Lebec, Stéphane Labrosse, Adrien Morison, Daniela P Bolrão, Paul J Tackley

► **To cite this version:**

Laëtitia Lebec, Stéphane Labrosse, Adrien Morison, Daniela P Bolrão, Paul J Tackley. Effects of salts on the exchanges through high-pressure ice layers of large ocean worlds. *Icarus*, 2024, 412, pp.115966. 10.1016/j.icarus.2024.115966 . hal-04823997

HAL Id: hal-04823997

<https://hal.science/hal-04823997v1>

Submitted on 6 Dec 2024

HAL is a multi-disciplinary open access archive for the deposit and dissemination of scientific research documents, whether they are published or not. The documents may come from teaching and research institutions in France or abroad, or from public or private research centers.

L'archive ouverte pluridisciplinaire **HAL**, est destinée au dépôt et à la diffusion de documents scientifiques de niveau recherche, publiés ou non, émanant des établissements d'enseignement et de recherche français ou étrangers, des laboratoires publics ou privés.

Copyright

Effects of salts on the exchanges through high-pressure ice layers of large ocean worlds

Laëtitia Lebec^{a,*}, Stéphane Labrosse^a, Adrien Morison^b, Daniela P. Bolrão^c and Paul J. Tackley^c

^aLGLTPE, ENS Lyon, Université Claude Bernard, 46 allée d'Italie, Lyon, 69364, France

^bPhysics and Astronomy, University of Exeter, Exeter, UK

^cDepartment of Earth Sciences, ETH-Zurich, Sonneggstrasse 5, Zurich, 8092, Switzerland

ARTICLE INFO

Keywords:

Satellites, dynamics

Ices

Interiors

Ganymede


ABSTRACT

The habitability of large icy moons has long been disputed due to the presence of an high-pressure (HP) ice layer located between the core and the internal liquid ocean, preventing a direct contact and facilitated exchanges between both. In our previous study [Lebec et al. \(2023\)](#), we have shown that under certain conditions and considering the phase change at the upper boundary of the HP ice shell, heat and mass transfer can occur and be efficient. Now, the aim of this work is to study the effects of impurities inside the HP ices on the flow dynamics and the mass transfer efficiency from the core to the ocean. These salts can enter the ice layer either by diffusion, which is a very inefficient process, or by partial melting at the bottom of the ice layer, if the temperature is high enough. In that case, the liquid water can interact with the core and get enriched in salts. This salts/water mixture, which can be lighter than high-pressure ices, could rise through the ice shell and refreeze. The resulting salts/ice mixture can be transported into the ocean by convection in the solid state but could also impede it due to its density compared to pure ice. Therefore, the convection efficiency depends on the buoyancy number B_{salts} , which is the ratio of density increase associated with salts compared to the decrease associated to temperature. To explore the impact of salts, we model a flux of salts from the core and the advection of these salts using Lagrangian tracers in order to study the effects of the Rayleigh number, the buoyancy number and K , which is the partition coefficient of the salts between the ocean and the HP ices at the top interface, on the heat and salts transfer efficiency through the HP ice layer, as well as the implications for the evolution of salt concentration in the ocean of large icy moons and ocean worlds. We present a scaling of the bottom temperature and the top radial velocity w_{top} as function of the Rayleigh number Ra_q for various values of the buoyancy number and a scaling of the effective flux of salts across the top interface with the ocean as function of the buoyancy number for various values of the partition coefficient. We perform a numerical application for Ganymede and show that depending on the values of the system parameters, a significant percentage of the salts entering the HP ice layer from the core can efficiently flow into the ocean.

1. Introduction

Large icy moons have a deep hydrosphere composed of a thin crust of ice Ih at the surface, a liquid ocean and a layer of high-pressure ices trapped between the ocean and the core ([Hussmann et al., 2015](#)). The internal oceans on Ganymede and Titan, which are the two largest moons of the solar system, are composed of salted water. For Ganymede, this has been inferred from electromagnetic measurements from the Galileo missions ([Kivelson et al., 2002](#)). For Titan, this has been deduced from gravity ([Iess et al., 2010, 2012; Mitri et al., 2014; Baland et al., 2014](#)), tides ([Iess et al., 2012](#)), rotation and shape ([Baland et al., 2014](#)) data from the Cassini mission and electromagnetic measurements from the Huygens probe ([Béghin et al., 2012](#)). These moons are mainly composed of rocks and ice and the composition of their rocky parts is likely to be close to carbonaceous chondrites ([Sotin et al., 2021](#)). According to [Zolotov and Kargel \(2009\)](#), their ocean's main salt is likely to be $MgSO_4$, which is compatible with the spectra obtained for Ganymede by the Galileo probe ([Soderlund et al., 2020](#)). These salts could be inherited from the formation and differentiation processes of the moon. They could also come from the core and reach the ocean by convection through the HP ice

*Corresponding author

 laetitia.lebec@ens-lyon.fr (L. Lebec)

ORCID(s): 0000-0001-8362-5142 (L. Lebec); 0000-0002-7620-4363 (S. Labrosse); 0000-0002-8261-9143 (A. Morison); 0000-0002-9509-9685 (D.P. Bolrão); 0000-0003-4878-621X (P.J. Tackley)

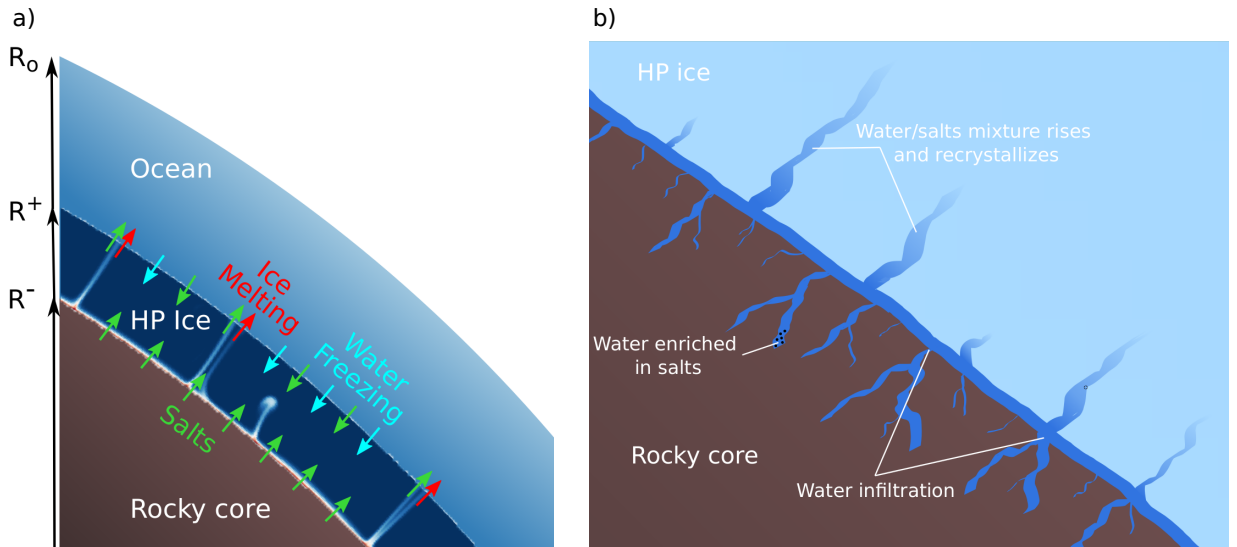


Figure 1: a. Model illustration for the interior of an ocean world with a compositional flux of salts from the core and exchanges of salts between the HP ice layer and the ocean. When the upwelling hot plumes reach the top interface between the ice and the ocean, the ice melts and the salts it contains dissolve in the ocean. Conversely, The water freezes above the downwelling currents and some of the salts it contains are trapped during crystallization, depending on the type of salts and the value of its partition coefficient between the water and the ice VI. b. Illustration of the process of enriching the HP ice layer with salts from the core. If there is melt at the interface between the HP ice layer and the rocky core, the liquid water will seep into the mantle and this interaction should enrich it with salts. If this salty water is less dense than the ice, it should penetrate into the HP ice layer by porous flow and rise until the temperature decrease along the way makes it recrystallize at a depth depending on the salts present in the water and the implied solidus.

layer (See Fig. 1.a), which would imply the presence of impurities also in this ice shell. In particular, if melting happens at the bottom of the ice layer in contact with the core (Kalousová et al., 2018; Choblet et al., 2017; Lebec et al., 2023; Kalousová and Sotin, 2018, 2020), the core interacts with the water which gets enriched in salts. If the salty water is less dense than the overlying ice (i.e. if the salt concentration is not too high), it is expected to penetrate in the ice by porous flow. In some conditions, this porous flow can proceed all the way to the ocean (Kalousová et al., 2018; Kalousová and Sotin, 2018, 2020) but, the decrease in temperature with height in the convective boundary layer leads to freezing of part, if not all, of the mixture in some cases (See Fig. 1.b). The resulting solid, likely a polycrystalline assemblage of salty ice and hydrated salts, is denser than pure ice. Some salts like NH_3 make the mixture less dense than pure ice (Leliwa-Kopystyński et al., 2002) and therefore help convection. We only consider here the adverse situation where salts make the density increase. This density increase counteracts the density decrease associated with temperature and the competition between these two effects controls the convective dynamics of the ice layer. This competition is quantified by a dimensionless parameter, classically called buoyancy number B_{salts} , which is the ratio between the density increase associated with salt enrichment and the density decrease associated with temperature increase. In addition to the possibility of salt transfer from the rocky core to the ocean, salts already present in the ocean can be transferred to the ice layer by freezing, provided that the partition coefficient K is greater than zero.

Hernandez et al. (2022) previously proposed a scaling to estimate whether the salts are impeding convection in the solid state. But despite the fact that the existence of a salty ocean is supported by several studies, a complete exploration of their effects on the mass and heat transfer efficiency through a HP ice layer inside large icy moons, depending on their buoyancy and their partition coefficient between HP ices and the ocean, has not yet been performed.

Several papers have already considered convection in high pressure ice layers of large icy moons: Choblet et al. (2017) modeled a 3D spherical ice layer with a pressure- and temperature-dependent viscosity of the ice. They also considered the ability of the ice to melt at the bottom interface and an instantaneous extraction of the melt to the ocean. Kalousová and Sotin (2018) and Kalousová et al. (2018) studied the evolution of a 2D cartesian HP ice layer. They treated the partial melting in the bulk and the transport of the melt across the ice shell with a variable viscosity

(Kalousová and Sotin, 2018; Kalousová et al., 2018; Kalousová and Sotin, 2020), using a two-phase approach. In a previous paper (Lebec et al., 2023), we modeled a two-dimensional spherical HP ice layer treating only solid-state convection for a constant viscosity (except for one case including a temperature- and pressure-dependent viscosity), but contrary to previous studies we considered the effect on the overall dynamics of the phase change (i.e. melting/freezing) at the interface between the ocean and the ice. Due to convective stresses in the ice, topography is formed at this interface. The topographic variations are partially erased by melting and freezing. This process implies a permeable boundary that enhances the heat and mass transfer efficiency through the top interface. It can be modeled as a phase change boundary condition controlled by a dimensionless parameter Φ . All these previous papers show that, depending on the heat flux from the core, the thickness of the ice and its viscosity, efficient heat and mass transfers may have existed, or may exist, through this layer. Furthermore, all of these studies have shown that under certain conditions, the temperature at the lower boundary between the core and the HP ice layer could reach the melting temperature, which would imply at least pockets of molten ice at the interface and a more efficient mass transfer through the ice shell, either by remaining liquid throughout ascent or by solid-state convection if water rises and refreezes in the ascending hot plumes during the ascent.

The present study, while still setting aside the question of two-phase flow, focuses on the effect of salts on the dynamics. We consider a flux of salts from the core and we use a numerical model to solve the convection equations. We perform a systematic exploration of the parameter space, which is composed of the Rayleigh number Ra_q , the phase change number Φ at the top boundary, the buoyancy number of the salts B_{salts} and the partition coefficient K of the salts between the liquid water and the HP ices at the top interface. The value of this coefficient depends on the nature of the salts. In the context of large ocean worlds, the first point is to know which salts could be dissolved in water by interacting with the core. Although partition coefficients of most salts between liquid water and ice Ih are well known, it is not the case when we consider water and high pressure ices (with the notable exception of NaCl, for which the partition coefficient is about 5×10^{-3} for ice VI, and about 0.12 for ice VII, according to Journaux et al. (2017)). We expect this coefficient to be rather low but, as it can vary a lot depending on the salt properties, we decided to use a wide range of values between 0 and 1 for this coefficient, $K = 1$ being a non-realistic maximum, in order to have the most comprehensive possible study of the environment so that the results are applicable when the salts involved are better identified and to determine their effect on the global dynamics.

Section 2 presents the physical model and the numerical method used in this study. The results are discussed in section 3, including a numerical application to Ganymede in subsection 3.4. The limits and perspectives of this work are discussed in section 4 and the results are summarized in section 5.

2. Model

In this study we consider a model made of a HP ice layer extending from R^- to R^+ topped by an ocean extending from R^+ to R_o (See Fig. 1.a) with fixed boundaries in time. Two fluxes are entering the HP ice layer from the core: the heat flux q and the compositional flux of salts F . The ocean is homogeneous by construction but evolves in time by exchanging mass with the HP ice layer. The ice transported by solid convection in the HP ice shell melts on contact with the ocean and the salts contained in the ice dissolve in it. Conversely, a part of the water near the upper interface between the HP ice and the ocean may freeze and be accreted to the ice (fig. 1.a). A certain amount of the salts present in the water during its crystallization is trapped in the process, depending on the salt partition coefficient K between HP VI ice and water. All these aspects are considered in our model.

2.1. Physical model

2.1.1. Governing equations

The primary target of our study is Ganymede but we aim at obtaining results that can apply to any object with a thick enough hydrosphere to host a high pressure ice layer. We therefore use dimensionless equations in order to reduce the number of parameters of the problem and obtain scaling laws for quantities of interest as function of these parameters. The length scale is taken as the HP ice layer thickness $d = R^+ - R^-$, with R^+ (resp. R^-) the dimensional radius of the top (resp. bottom) HP ice boundary. Therefore, in the following, the dimensionless radial coordinate defined as $(r - R^-)/d$ varies between 0 and 1. The radius ratio between the core and the HP ice layer is $\gamma = R^-/R^+$. The time scale is defined using the thermal diffusivity κ as d^2/κ . As in previous papers on convection in HP ice layers (Choblet et al., 2017; Kalousová et al., 2018; Lebec et al., 2023), we impose a heat flux q at the bottom of the layer and it is used to scale the temperature with $\Delta T = qd/k$, with k the thermal conductivity. Also, the temperature T^+ at the interface

131 between the HP ice and the ocean is set to the melting one at the relevant depth, which depends on the HP ice layer
 132 thickness d . The temperature is made dimensionless using the following equation:

$$\tilde{T} = k \frac{T - T^+}{qd}. \quad (1)$$

133 In addition to the temperature, another scalar field is considered in this paper, the mass fraction of salts C (or
 134 concentration). Note that the salt concentration we consider is that for the “fluid parcel” which constitutes the basic
 135 element of the hydrodynamics approach used here, which is much larger than the typical grain size of the solid. The
 136 salts do not need to be dissolved in the ice crystals and can be in the form of separate crystals. In that sense, the mineral
 137 assemblage is similar to the one that forms the rocks constitutive of the mantle of terrestrial planets. As long as they
 138 stay in the solid state, the various crystals cannot segregate.

139 In a first set of runs (see Table 1 #1), we consider a closed ice/ocean system without an influx of salts from the core
 140 and with an initial concentration in the ocean $C_{ini}^o = 1$ as the scaling variable. In a second set of runs (see Table 1 #2),
 141 we impose a fixed flux of salts at the bottom of the ice layer, F (unit of m s^{-1}) which is used to scale the concentration
 142 so that the dimensionless salt flux imposed at the bottom is $F_{salts} = 1$. To impose a fixed flux of salts, we assume an
 143 infinite supply of salts from the core (This point is raised in the discussion § 4).

144 This problem is solved in a spherical shell under the Boussinesq approximation for an infinite Prandtl number.
 145 Indeed, from values in Table 4 in the case of Ganymede:

$$Pr = \frac{\eta}{\rho\kappa} \sim 10^{20}, \quad (2)$$

146 with ρ the reference density and η the ice viscosity. In this study, η is considered constant throughout the HP ice shell.
 147 The dimensionless conservation equations of mass, momentum, energy and composition are (Tackley and King, 2003;
 148 Bolrão et al., 2021):

$$\nabla \cdot \mathbf{u} = 0, \quad (3)$$

$$0 = -\nabla p + \nabla^2 \mathbf{u} + Ra_q (T - \bar{T} - B_{salts}(C - \bar{C})) \hat{\mathbf{r}}, \quad (4)$$

$$\frac{\partial T}{\partial t} + \mathbf{u} \cdot \nabla T = \nabla^2 T, \quad (5)$$

$$\frac{\partial C}{\partial t} + \mathbf{u} \cdot \nabla C = 0, \quad (6)$$

149 with $\hat{\mathbf{r}}$ the radial unit vector, p the dynamic pressure, $\mathbf{u} = (v, w)$ the velocity, \bar{T} the horizontally averaged temperature,
 150 \bar{C} the horizontally averaged concentration in salts, and Ra_q the Rayleigh number. In our case of a fixed heat flux from
 151 the core and a laterally-varying temperature at the interface between the HP ice and the core, Ra_q is written as (Choblet
 152 et al., 2017):

$$Ra_q = \frac{\alpha \rho g q d^4}{k \kappa \eta}, \quad (7)$$

153 with g the gravity acceleration and α the thermal expansion.

154 The equation (6) for the evolution of the concentration in salts is a pure advection equation, i.e. we neglect its
 155 diffusion in the ice. Its effect on the ice density is controlled by a dimensionless number, the buoyancy number, which
 156 is the ratio of density increase associated to salts $\Delta\rho^c$ compared to the decrease associated to temperature, $\Delta\rho^T = \rho\alpha\Delta T$
 157 (Le Bars and Davaille, 2004). With $\Delta T = qd/k$, in the case of a closed ice/ocean system without influx of salts from
 158 the core, this parameter is written as:

$$B_{salts} = \frac{\Delta\rho^c}{\Delta\rho^T} = \frac{kKC_{ini}^o}{\alpha qd} = \frac{kK}{\alpha qd}, \quad (8)$$

159 while in the case of an imposed flux of salts F from the core, it is written as:

$$B_{salts} = \frac{\Delta\rho^c}{\Delta\rho^T} = \frac{kF}{\alpha \kappa q}. \quad (9)$$

The latter expression is obtained using the Fd^2/κ as scale for the variations of composition, as dictated by equation (6) and the use of thermal diffusion to scale times. A negligible value of B_{salts} would make the flow insensitive to the presence of salts, irrespective of its concentration, while a large value would tend to make salt-enriched regions negatively buoyant and possibly stable against thermal convection. One of the goals of the present paper is precisely to explore the effects of this parameter on the dynamics of convection in a HP ice layer and resulting transfer efficiency.

The buoyancy number is controlled by the nature of the salts and their amount expected to enter the ice layer if melting occurs at the bottom. These difficult questions depend on the initial composition of the ocean and its chemical interactions with the underlying rocky core, which depend on the pressure and temperature. To our knowledge, the relevant studies are scarce and let us here consider the case of NaCl for which some data exist (Journaux et al., 2013, 2017). The maximum amount of NaCl for our model to hold is the one that makes the salty water negatively buoyant, since we need it to rise in the ice to freeze. This maximum concentration is $2.5 \text{ mol kg}_{H_2O}^{-1}$ (Journaux et al., 2013) or $146 \text{ g kg}_{H_2O}^{-1}$, which means that liquid water at high pressure can contain a maximum of about 15 wt.% of NaCl to be able to rise through the HP ice layer. According to Journaux et al. (2017), the concentration of NaCl in ice VI cannot exceed $2.1 \times 10^{-2} \text{ mol\%}$, or $5.6 \text{ g kg}_{iceVI}^{-1}$. Any additional salts contained in the water would crystallise as salt grains. According to Kalousová et al. (2018), under conditions consistent for Ganymede, the water fraction in the ice layer could be up to 1% and its radial velocity at top is of the order of a few meters per year. Assuming that the radial velocity in the bulk is slightly lower but of the same order of magnitude as that at the top, say 1 m yr^{-1} , we can estimate the maximum flux of NaCl across the HP ice shell at a given time. This flux depends on the maximum concentration of NaCl in the water at high pressure (15 wt.%), the maximum fraction of liquid in the layer at a given time (0.01) and the radial velocity of the water and salts mixture through the ice ($3.2 \times 10^{-8} \text{ m s}^{-1}$), which gives, as their product, $F = 4.8 \times 10^{-11} \text{ m s}^{-1}$. Based on this estimate, we can compute the maximum buoyancy number from eq. 9 in order to chose wisely the range to be used for this study. For Ganymede, using the values available in Table. 4, this gives $B_{salts} < 60$. Therefore, we chose a range between 0 and 10, which is sufficiently large to cover the whole range of behaviour, as shown below.

2.1.2. Boundary conditions

Our model uses a fixed heat flux from the rocky core and the temperature is therefore free to vary laterally and on average at the bottom of the studied shell. At the interface between the HP ice and the ocean, the temperature is equal to the liquidus of the overlying ocean assumed to be laterally uniform so that, according to equation (1), the dimensionless temperature is set to zero, leading to the following dimensionless temperature top (+) and bottom (-) boundary conditions:

$$\begin{cases} \tilde{T}^+ = 0 \\ \left(\frac{\partial \tilde{T}}{\partial r}\right)^- = -1, \end{cases} \quad (10)$$

The mechanical boundary condition that applies at the bottom of the HP ice layer is not obvious (see discussion in Lebec et al., 2023): if the bottom temperature is below the solidus, the whole shell is solid and the contact with a high viscosity rocky core implies a no-slip boundary condition. On the other hand, in the case of a thick ice layer, the bottom temperature is likely to reach the melting temperature of the HP ice, in places (the temperature being laterally variable) or everywhere. In the extreme case where a liquid is present everywhere between the ice and the core, we can expect a free-slip boundary to apply. Intermediate possibilities with a Robin-like boundary condition, which could be laterally variable as a function of the local temperature, could be envisioned. As shown by Lebec et al. (2023), heat and mass transfer is more efficient for a free-slip bottom boundary condition and, to be on the conservative side, we consider a no-slip boundary condition in the present study:

$$u^- = w^- = 0. \quad (11)$$

The presence of a solid-liquid phase change at the upper boundary of the ice shell imposes a specific boundary condition with important implications for the dynamics and the heat and mass transfer efficiency. The detailed derivation and implications of this boundary condition for Rayleigh-Bénard convection can be found in several papers (Deguen, 2013; Deguen et al., 2013; Labrosse et al., 2018; Agrusta et al., 2020; Bolrão et al., 2021). The convection pattern inside a HP ice layer with such a boundary condition at the top (Lebec et al., 2023) is made of upwelling hot plumes and a diffuse downwelling current, as shown on top panels of Fig.8. At the interface with the ocean, the

205 upwelling hot ice plumes melt and join the ocean while a part of the liquid water can solidify and accrete to the ice
 206 above the downwelling cold flow. The ease with which this process occurs depends on the competition between two
 207 processes: on the one hand, the convective stresses in the solid create topography at the interface. On the other hand,
 208 convection in the ocean erases this topography by melting and freezing. This competition is quantified by the ratio of
 209 the two relevant time scales, the one to build the topography, which is:

$$\tau_{\eta} = \frac{\eta}{\Delta\rho g d}, \quad (12)$$

210 with $\Delta\rho = \rho_s - \rho_l$ the density difference between the solid (ρ_s) and the liquid (ρ_l) at the interface, and the one to erase
 211 it by melting and freezing, which is:

$$\tau_{\phi} = \frac{\rho_s L}{\rho_l c_{pl} u_l \left| \frac{\partial T_m}{\partial r} \right|}, \quad (13)$$

212 with L the latent heat, u_l the flow velocity in the liquid ocean, c_{pl} the specific heat of the liquid and $\partial T_m / \partial r$ the slope
 213 of melting temperature with radius (see [Labrosse et al., 2018](#), for a full treatment of this process). Therefore, the phase
 214 change number, defining the efficiency of this mechanical condition, is written as:

$$\Phi = \frac{\tau_{\phi}}{\tau_{\eta}}. \quad (14)$$

215 Expressing the continuity of stress across the boundary leads to the dimensionless boundary condition for the radial
 216 velocity associated with the phase change considered at the top interface:

$$\Phi w + 2 \frac{\partial w}{\partial r} - p = 0. \quad (15)$$

217 When $\Phi \rightarrow 0$ the timescale to erase the topography is much lower than the one to create it and the phase change is
 218 efficient at the interface. While for $\Phi \rightarrow \infty$, we fall back on the classical non-penetrative boundary condition and the
 219 radial velocity at the interface tends to zero, which implies a very inefficient mass transfer between the ice and the
 220 ocean. In this study, cases assume an efficient phase change of $\Phi = 10^{-2}$, which gives the dynamical regime expected
 221 for large rich-water bodies ([Lebec et al., 2023](#)).

222 The equation (6) for the composition being hyperbolic, no boundary condition can be applied and a specific
 223 treatment is needed to impose an influx of salts at the bottom. As discussed below in section 2.2.2, this is done using
 224 Lagrangian tracers. At the bottom of the ice layer, we impose an influx of salts corresponding to a dimensionless flux
 225 per surface area $F_{salts} = Fd/\kappa = 1$. At the upper boundary, there is a mass exchange between the ice and the ocean
 226 by the solid-liquid phase change, as a result of the mechanical boundary condition just discussed. This mass exchange
 227 is treated differently on both sides. At regions of downflow in the ice, water freezes to form newly accreted ice whose
 228 composition is set by the partition coefficient, K , as $K C^o$, with C^o the concentration of salts in the ocean (Fig. 2).
 229 Where ice is flowing toward the ocean, it must reach an equilibrium, which implies a modification of its temperature
 230 by diffusion and complete melting, irrespective of its composition (Fig. 2). The liquid is at the liquidus corresponding
 231 to its composition, which could be different from the solidus corresponding to the composition of the solid. In most
 232 cases, the solidus of the solid is likely lower than the liquidus of the liquid, in particular if the phase diagram presents
 233 a eutectic. In that case, melting of ice is eased, and it could even start before reaching the boundary ([Kalousová et al.,
 234 2018](#)), a possibility not treated in the present study. If, on the other hand, the liquidus of the liquid is lower than the
 235 solidus of the solid, the excess salt in the liquid serves as fusing agent, similarly to the salt spread on snowy roads in
 236 mountain regions. In both cases we therefore expect the whole ice flowing through the boundary to melt and its content
 237 to mix with the ocean.

238 2.1.3. Evolution of the ocean composition

239 As explained in the introduction to this section, the ocean evolves in time through mass exchanges with the HP ice
 240 layer. The concentration of salts in the ocean C^o evolves over time as:

$$M^o \frac{dC^o}{dt} = 4\pi(R^+)^2 \rho F^o, \quad (16)$$

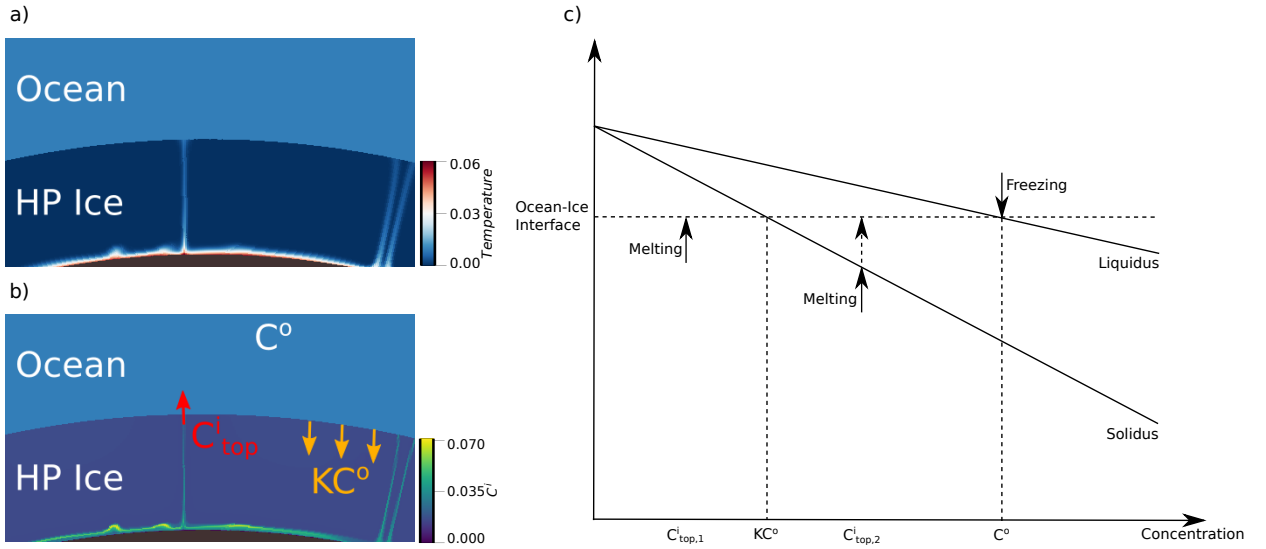


Figure 2: Illustration of the treatment of the composition at the interface between the HP ice layer and the ocean. a) Snapshot of the temperature field in the HP ice layer. b) Snapshot of the composition field in the HP ice layer. c) Phase diagram near the interface between the HP ice layer and the ocean (see text for details). It displays two options for C_{top}^i , which is the concentration of salts in the upwelling hot plumes near the interface. If $C_{top}^i > KC^o$, the ice starts to melt at the solidus, under the interface with the ocean, i.e. at a temperature below that of the interface. If $C_{top}^i < KC^o$, melting occurs directly at the ice-ocean interface, due to the reaction with highly salted water.

241 with F^o the total flux of salts at the interface between the ice and the ocean in m s^{-1} (and ρF^o the total mass flux in $\text{kg m}^{-2} \text{s}^{-1}$) and $M^o = (4/3)\pi(R_o^3 - (R^+)^3)\rho$ the ocean mass.

243 The total flux of salts F^o from the ice to the ocean is composed of an inward flux and an outward flux. The salt/ice mixture transported in the upwelling hot plumes reaches the interface with a radial velocity at top $w_{top} > 0$ and the ice melts at this contact. In this case, the salts contained in the ice melting at the interface are transported from the ice to the ocean. Conversely, above the downwelling currents $w_{top} < 0$ and a certain amount of salts depending on K enters the ice due to freezing at the boundary (See Fig. 2). The expression of this flux depends on the value of the top radial velocity as:

$$F^o = \begin{cases} w_{top} C_{top}^i & \text{if } w_{top} > 0 \\ w_{top} KC^o & \text{if } w_{top} < 0. \end{cases}$$

249 with C_{top}^i the concentration of salts in the ice that melts at the interface.

250 2.2. Numerical method

251 2.2.1. Numerical solution

252 In this study we used StagYY (Tackley, 2008) to solve the convection equations (§ 2.1.1) subject to boundary conditions described in section § 2.1.2. The geometry considered for this model is a two-dimensional spherical annulus (Hernlund and Tackley, 2008). This convection code, originally developed for convection in rocky mantles, solves the convection equations in various geometries using a finite volume approach and uses Lagrangian tracers to treat composition (as discussed below). The longitudinal aperture on which the convection equations are solved is set to $\frac{\pi}{6}$ in all cases, which is enough to capture at least one horizontal period (Lebec et al., 2023). We impose periodicity in the longitudinal direction. For the grid, we choose the number of cells in the radial direction $n_{z_{tot}} = 128$ in order to have a high enough resolution to reach the global energy balance. The number of cells in the horizontal direction $n_{y_{tot}}$ is computed in order to make the cells as square as possible. Therefore, for the runs with a radius ratio $\gamma = 0.8$, $n_{y_{tot}} = 256$ and for $\gamma = 0.9$, $n_{y_{tot}} = 512$. As we will see in the results, in some cases the salts accumulate at the bottom

262 of the HP ice layer. Therefore, the grid is refined in the radial direction by a factor of 6 near the core/ice interface. It is
 263 also refined by a factor of 2 near the top boundary to properly solve the phase change.

264 Another numerical issue regards high Rayleigh numbers. All the runs of this work are for a Rayleigh number
 265 between 10^7 and 10^9 and an efficient phase change $\Phi = 10^{-2}$ at top. Due to this phase change, the thermal boundary
 266 layer at the top interface is $1/w_{top}$ thick. Knowing that the radial velocity at top can be very high, these runs require
 267 a very small grid spacing near the interface to be resolved correctly. To this end, we adopt an approach developed
 268 by [Agrusta et al. \(2020\)](#) and used by [Lebec et al. \(2023\)](#) which removes the thin boundary layer and applies a Robin
 269 boundary condition, which allows us to switch from a fixed flux boundary condition to a fixed temperature boundary
 270 condition along the interface depending on the value of the radial velocity. This condition is written as ([Agrusta et al.,](#)
 271 [2020](#)):

$$\Gamma T + (1 - \Gamma) \frac{\partial T}{\partial r} = 0. \quad (17)$$

272 Γ is the following approximation of the Heaviside function:

$$\Gamma = \frac{1}{2} \left[1 + \tanh \left(\pi \frac{\frac{w_0}{2} - w_{top}}{\frac{w_0}{2}} \right) \right], \quad (18)$$

273 with w_0 the velocity threshold between both conditions, chosen here as $w_0 = 5 \times 10^{-2} Ra_q^{2/3}$. Depending on the value
 274 of w_{top} , representing the upwelling hot plumes and downwelling currents velocity at the interface, this function makes
 275 the boundary condition change smoothly from a Neumann boundary condition for which $\frac{\partial T}{\partial r} = 0$ in fast upwelling
 276 regions to a Dirichlet boundary condition for which $T = 0$ in downwelling or slowly upwelling regions.

277 2.2.2. Compositional tracers of salts

278 To explore the effect of salts on the heat and mass transfer through a HP ice layer, we use Lagrangian tracers
 279 distributed throughout the ice shell ([Tackley and King, 2003](#), for more information on the use of tracers and
 280 benchmarking). These tracers carry the composition in salts of the HP ice layer. At each time step, the information
 281 carried by the tracers is used to compute a salt concentration field on the finite volume grid which, together with the
 282 temperature field, is used to compute the total buoyancy force on the right-hand-side of equation 4. Using a finite
 283 volume approach, the code solves the flow velocity, which is then used to compute the evolution of temperature and
 284 composition.

285 As explained before, if the bottom temperature is high enough to melt the ice, the water in contact with the core
 286 gets enriched in salts. If this mixture is less dense than the ice, it should rise through the HP ice shell by porous
 287 flow and recrystallize. Then, the salts/ice mixture obtained could reach the ocean by convection in the solid state. This
 288 process of porous flow requires a full two-phase flow treatment to be modeled self-consistently ([Kalousová et al., 2018](#)).
 289 Alternatively, we chose to impose a salt flux at the boundary. However, in the absence of salt diffusion in equation (6),
 290 applying a boundary condition does not affect the solution. We adopt the approach proposed by [Bouffard et al. \(2017\)](#)
 291 to model this compositional flux: we add a concentration $\delta C(r)$ corresponding to the desired flux directly to the tracers
 292 as

$$\int_{r^-}^{r^+} r^2 \delta C(r) dr = r^{-2} F_{salts} \Delta t, \quad (19)$$

293 with r^- (resp. r^+) the dimensionless radius of the bottom (resp. top) boundary of the HP ice layer, knowing $r^+ - r^- = 1$,
 294 F_{salts} the dimensionless flux of salts per surface unit and Δt the time step. This additional concentration is added
 295 following a Gaussian-like curve centered around a horizontal line just above the bottom interface, as follows:

$$\delta C(r) = \frac{a_F \Delta t}{r^2} \exp \left(-\frac{(r - (r^- + h))^2}{\sigma^2} \right), \quad (20)$$

296 with $h = 0.05$ the position of the peak above the bottom boundary and $\sigma = 0.01$ the peak thickness (the values have
 297 been chosen empirically), r the position of the tracer inside the HP ice layer to which we add δC and a_F a constant

Table 1

All simulations are done for a rigid bottom boundary condition and an efficient phase change at top $\Phi = 10^{-2}$. \bullet^o is for ocean and \bullet^i is for the HP ice layer. C_{ini} is the initial concentration of salts in the designated shell.

#	F_{salts}	C_{ini}^o	C_{ini}^i	K	B_{salts}	Ra_q	γ
1	0	1	0	{0.001, 1}	{0, 3, 10}	10^7	{0.8, 0.9}
2	1	0	0	{0, 0.001, 0.01, 0.1, 0.3, 1}	{0, 0.1, 0.3, 1, 3, 10}	{ $10^7, 10^8, 10^9$ }	{0.8, 0.9}
				0.01	{0, 0.1, 0.3, 1, 3, 10}	{ $3 \times 10^7, 3 \times 10^8$ }	0.8
				0.01	0.5	{ $10^7, 2 \times 10^7, 3 \times 10^7, 6 \times 10^7, 10^8, 2 \times 10^8, 3 \times 10^8, 6 \times 10^8, 10^9$ }	{0.8, 0.9}

298 computed from eq. 19 as:

$$a_F = \frac{2(r^-)^2 F_{salts}}{\sqrt{\pi} \sigma \left(\operatorname{erf} \left(\frac{1-h}{\sigma} \right) + \operatorname{erf} \left(\frac{h}{\sigma} \right) \right)}. \quad (21)$$

299

300

301

302

303

304

Because of the way the flux of salts from the core is modeled, with a concentration distributed in the ice layer according to a Gaussian-like curve, the number of tracers per cell has to be large enough to ensure the smallest possible error on the imposed flux. After some computation to optimize the flux quality/computational resources ratio, we fixed it at 500 tracers per cell.

305 3. Results

306

307

308

309

310

311

312

313

314

315

316

317

318

319

320

321

322

323

Two sets of runs have been performed in order to study the effect of salts in the most systematic way, as listed in Table 1. Firstly, we performed a few runs (#1) with a zero salts flux from the core and a non-zero initial salt concentration $C_{ini}^o = 1$ in the ocean to study whether an equilibrium is reached between the ocean and the HP ice layer in terms of composition and the time required to reach a steady state in a closed ocean/HP ice system. As listed in Table 1, we chose various values of B_{salts} between 0 and 10. Applying eq. (8) to Ganymede with $K \in [0, 1]$ and values for q and d in Table 4, we get B_{salts} in the range 0 to 5. In order to cover all possibilities, in particular when considering other planetary objects, we explore values of B_{salts} up to 10, which is sufficient to exhibit all dynamical outcomes.

For the second set (#2) we added a compositional flux of salts $F_{salts} = 1$ at the bottom of the HP ice layer. Therefore, the runs never reach a steady-state because the salts continuously enter the ice and the concentration of salts increases with time. These runs all start with a zero initial concentration of salts in the ocean C_{ini}^o , and in the HP ice layer C_{ini}^i and are performed for large ranges of values for K , B_{salts} , Ra_q and for two values of the radius ratio γ . We vary B_{salts} systematically to cover all dynamical regimes. As listed in Table 1, we chose various values of B_{salts} between 0 and 10. If we apply eq. (9) to Ganymede, depending on the value chosen for q in Table 4, we obtain a range for F between 0 and $1.6 \times 10^{-11} \text{ m s}^{-1}$.

An alternative way to view the choice of parameters B_{salts} is to compute the value of $\Delta\rho^c$ corresponding to $B_{salts} = 1$. From eq. (8) and eq. (9), $\Delta\rho^c / \rho_{H_2O} = \alpha q d / k$. For the total range of values for Ganymede (Tab. 4), we get $\Delta\rho^c / \rho_{H_2O}$ between 0.19 and 1.7. Assuming a mechanical mixture between salt and HP ice, we can compute the mass fraction of salts X_m as:

$$X_m = \frac{M_{salts}}{M_{H_2O}} = \frac{\frac{\Delta\rho^c}{\rho_{H_2O}} \frac{\rho_{salts}}{\rho_{H_2O}}}{\frac{\rho_{salts}}{\rho_{H_2O}} - \frac{\Delta\rho^c}{\rho_{H_2O}} - 1}. \quad (22)$$

324

325

326

Considering for example NaCl, $\rho_{salts} / \rho_{H_2O} \simeq 2.17$. Therefore, $X_m = 0.42$ for $\Delta\rho^c / \rho_{H_2O} = 0.19$ but $\Delta\rho^c / \rho_{H_2O} = 1.7$ gives an unacceptable negative value for X_m . This shows that some combinations of parameters are not physically possible for all types of salts. We can also compute the density of salts for the limit case $X_m = 1$ as:

$$\frac{\rho_{salts}}{\rho_{H_2O}} = \frac{1 + \frac{\Delta\rho^c}{\rho_{H_2O}}}{1 - \frac{\Delta\rho^c}{\rho_{H_2O}}}. \quad (23)$$

327 For $\Delta\rho^c/\rho_{H_2O} = 0.19$, the minimum density of salts acceptable for the mass concentration of salts to be inferior to 1
 328 is $\rho_{salts}/\rho_{H_2O} = 1.47$.

329 3.1. Closed ocean/HP ice system

330 Before imposing a flux of salts from the core, let us study the evolution of a closed ocean/HP ice system (See study
 331 case #1 in Table 1). Without an influx of salts from the core, the two layers evolve according to two parameters: B_{salts}
 332 and K until reaching a steady-state after a certain amount of time. If the system reaches an equilibrium, the two layers
 333 are balanced, each around an equilibrium concentration. A similar study was performed by Bolrão et al. (2021) but
 334 with different boundary conditions and geometry, relevant to the magma oceans on Earth.

335 Starting with a zero concentration in the HP ice shell, we set an initial concentration of salts in the ocean $C_{ini}^o = 1$.
 336 If the whole ice layer reaches an equilibrium with the ocean (which is homogeneous by construction of the model), the
 337 concentration in the ocean tends to C_{eq}^o and the one in the ice tends to C_{eq}^i , both expressed from the initial concentration
 338 C_{ini}^o , the partition coefficient K and the volumes of both layers as:

$$C_{eq}^o = C_{ini}^o \frac{V^o}{V^o + KV^i}, \quad (24)$$

339

$$C_{eq}^i = KC_{eq}^o = C_{ini}^o \frac{KV^o}{V^o + KV^i}, \quad (25)$$

340 with V^i (resp. V^o) the volume of the HP ice layer (resp. ocean).

341 Figure 3 shows the evolution of the concentration in salts of the ocean (top panels) and of the ice (bottom panels)
 342 for two partition coefficient values. These graphs are made for various values of the buoyancy number and the red line
 343 shows the equilibrium concentrations C_{eq}^o in the ocean and C_{eq}^i in the ice. Figure 4 shows snapshots of 1/12 of the
 344 HP ice layer at the end of the runs for some of these cases. For both $K = 10^{-3}$ and $K = 1$, the concentration of salts
 345 in the ocean decreases as it increases in the ice due to the development of convection. For small values of B_{salts} , the
 346 salts incorporated in the ice in the early stage are entrained back to the ocean which makes its concentration rebound.
 347 These two processes eventually balance each other out and the system reaches steady-state. For a partition coefficient
 348 of 1 (see Fig. 3.a), all salts present in the water at the time of its recrystallization at the ocean/ice interface are trapped
 349 in the ice, leading from equations 25 and 24 to an equal value in both layers of the equilibrium concentration of salts
 350 at steady-state. This is what happens in the case $B_{salts} = 0$, for which both concentrations tend to their equilibrium
 351 values (eqns. 24 and 25). The salts are easily transported from one layer to another, leading at steady-state to an almost
 352 homogeneous HP ice layer, as can be seen on Fig. 4.a. However, these equations do not take into account the effect of
 353 the buoyancy number. Contrary to the ocean, the HP ice shell is not homogeneous and for $B_{salts} \geq 0.5$, salts from the
 354 ocean accumulate at the bottom of the HP ice layer. This effect can be observed in Fig. 4.b, in which the concentration
 355 is higher in the bottom part of the HP ice shell. Therefore, the salts are difficult to transfer to the ocean by convection
 356 and it leads, for $B_{salts} \geq 0.5$, to a mean concentration in the ice larger than the equilibrium value and lower than
 357 the equilibrium value in the ocean. The time required to evolve halfway to the steady-state concentration is reported
 358 in Table 2 and named $t^{1/2}$. It shows that, for $K = 1$, the higher the buoyancy number, the faster the steady state is
 359 reached. Contrary to all other cases displayed on Fig. 4, the temperature field in the HP ice layer for $B_{salts} = 10$ and
 360 $K = 1$ (see Fig. 4.b) shows that convection stopped. In this study, B_{salts} is an imposed input parameter that is not
 361 representative of what will be achieved in the run in terms of concentration and temperature contrast. A posteriori, an
 362 effective buoyancy number B_{eff} can be computed based on what has actually been achieved during the run, defined
 363 as:

$$B_{eff} = \frac{C_{bot}^i - C_{top}^i}{\tilde{T}_{bot} - \tilde{T}_{top}} B_{salts}. \quad (26)$$

364 In the case of Fig. 4.b, $B_{eff} = 20$, which is very high such that convection was impeded by the salts stacking at the
 365 bottom of the HP ice layer, unlike other cases for which the effective buoyancy number is in the range 0–0.1. To better
 366 understand this particular case, Figure 5 shows the evolution in time of the temperature and the concentration fields
 367 from an early stage of the run to $t = 4 \times 10^{-2}$, which is the time of Figure 4.b. On Fig. 5.a the convection is very strong
 368 and the buoyancy number is around 10. At this stage, the heavy salts enter the ice layer from above and therefore help

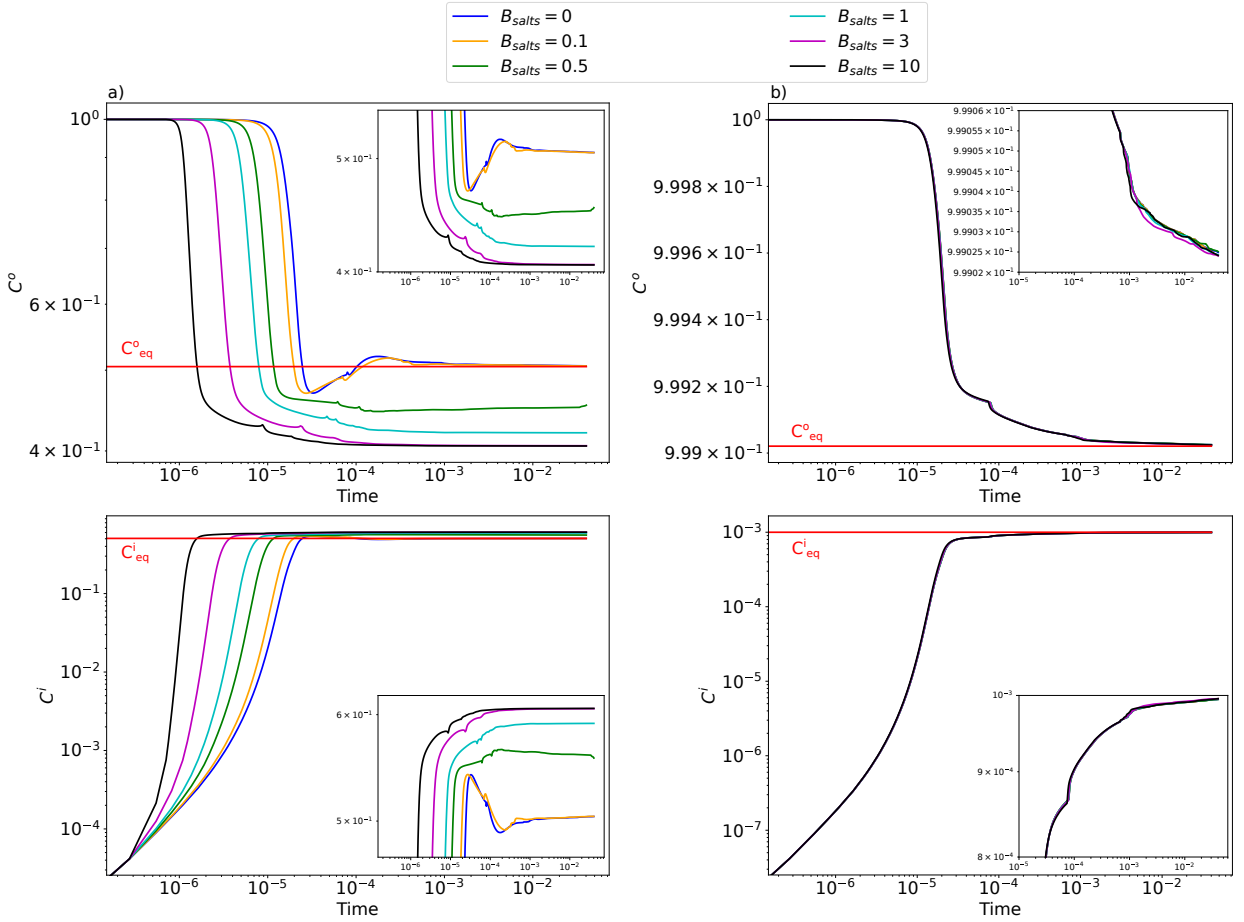


Figure 3: Evolution of the concentration in salts of the ocean (top) and the HP ice layer (bottom) with time for a partition coefficient a) $K = 1$ and b) $K = 10^{-3}$, a Rayleigh number $Ra_q = 10^7$, a radius ratio $\gamma = 0.8$ and various values of B_{salts} , as labeled.

369 convection, which is very fast. The salts are entering the layer above the downwelling currents and the upwelling hot
 370 plumes are poor in salts. At the time of Fig. 5.b, salts have already accumulated at the bottom of the ice layer and the
 371 effective buoyancy number is around 60, which is enough to inhibit convection. From that point, the salts continue to
 372 enter the ice from the ocean and build up at the bottom of the ice layer until the convective movements disappear.

373 For a low partition coefficient $K = 10^{-3}$ (see Fig. 3.b), the chosen buoyancy numbers have a very small impact on
 374 the dynamics because the concentration of salts trapped in the ice during freezing of water at the ice/ocean interface
 375 is very low. In that case, the effective buoyancy number for $B_{salts} = 10$ is $B_{eff} = 0.1$. This means that even for high
 376 values of B_{salts} the salts hardly affect the ice density and are still easily transported by convection. This can be observed
 377 in Fig. 4.c and Fig. 4.d which both show an almost homogeneous HP ice layer with the same concentration of salts
 378 in the bulk. This confirms that for a very small amount of salts entering the ice from the ocean in a closed ocean/HP
 379 ice system the salts do not accumulate at the bottom of the ice shell even for $B_{salts} = 10$. In all three cases shown in
 380 Fig. 4.a,c,d the HP ice layer is almost homogeneous except for a salts-poor thin layer near the lower interface. This is
 381 due to the rigid bottom boundary condition, which strongly inhibits vertical flow toward the boundary compared to the
 382 case of a free-slip boundary condition. In the case of a low partition coefficient, the salts concentrations in the ocean
 383 and in the ice layer tend to their respective equilibrium values, C_{eq}^o and C_{eq}^i , irrespective of the buoyancy number, but
 384 the equilibrium concentration in the ice is K times smaller than that in the ocean. Also, the time $t^{1/2}$ to reach half the

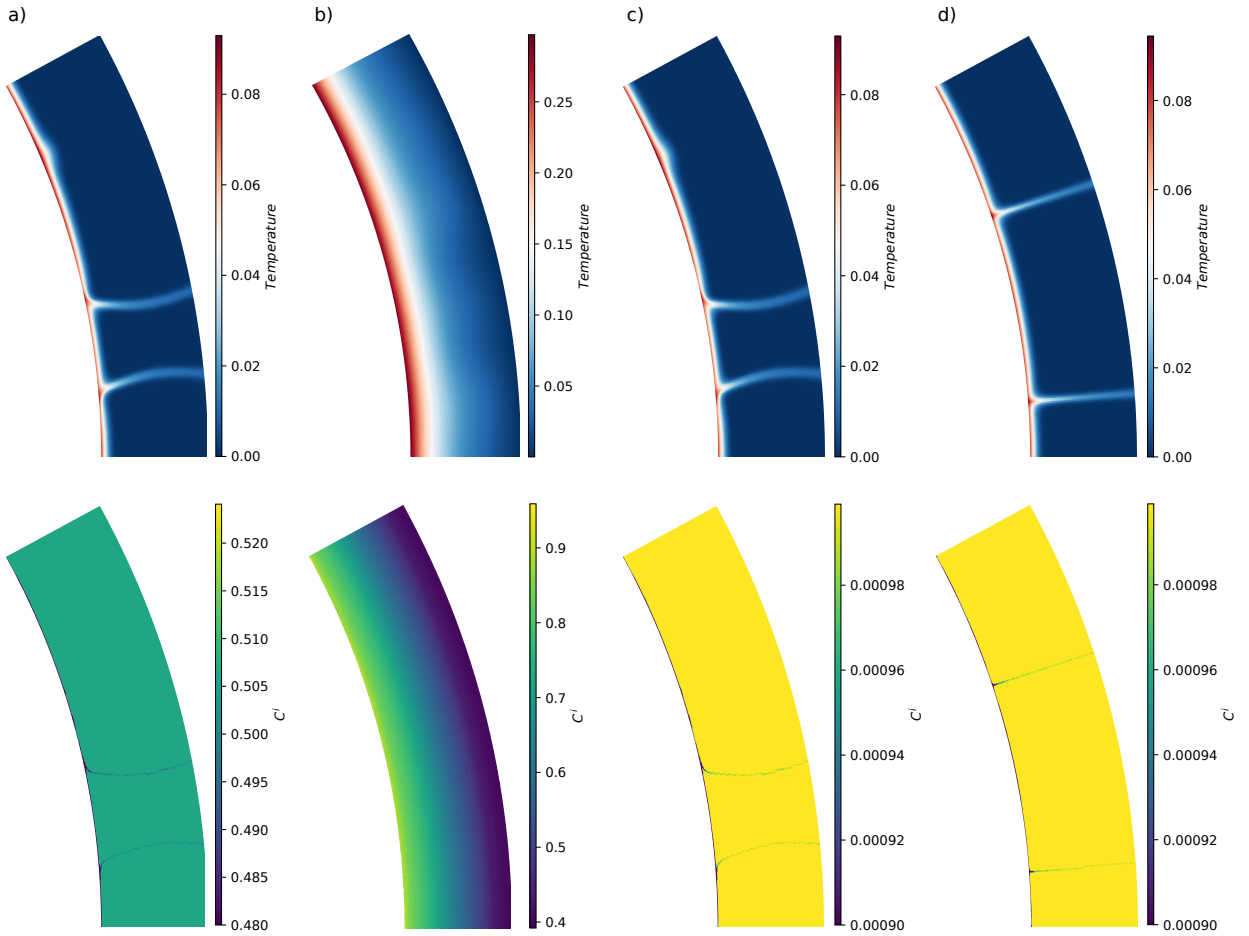


Figure 4: Snapshots of 1/12 of the HP ice layer in steady-state at $t \simeq 4 \times 10^{-2}$ for a Rayleigh number $Ra_q = 10^7$, a radius ratio $\gamma = 0.8$. The top (resp. bottom) panels show the temperature (resp. composition) inside the ice shell for a) $K = 1$ and $B_{salts} = 0$, b) $K = 1$ and $B_{salts} = 10$, c) $K = 10^{-3}$ and $B_{salts} = 0$ and d) $K = 10^{-3}$ and $B_{salts} = 10$. The minimum concentration of salts in the HP ice layer for a), c), d) is 0 but the color bars have been limited to a) 0.48 and c) & d) 9×10^{-4} in order to have more information about what happens in the bulk of the ice shell. Note that colorbars differ between panels.

385 steady-state concentration is the same whatever the buoyancy number considered in this study, because B_{eff} is close
 386 to zero in all of those cases. (See Table 2).

387 For all values of B_{salts} and K considered in this set of runs, the time to reach half of the steady-state concentration
 388 is in the range $10^{-6} - 10^{-5}$ (See Table 2). For Ganymede, using the values in Table 4, $t^{1/2}$ is of the order 1.5×10^4
 389 1.5×10^5 years.

390 3.2. Effects of an influx of salts on the overall dynamics

391 Now, adding a flux of salts from the core, we will discuss how the qualitative evolution of the system with time
 392 depends on the parameters B_{salts} and K , before discussing the two main regimes of salts transport through the HP
 393 ice layer as a function of the buoyancy number.

394 3.2.1. Qualitative effects of B_{salts} and K on the evolution of the system

395 In the rest of the results section, we analyse the runs of the study case #2 detailed in Table 1, starting with
 396 a qualitative analysis of the effects of the buoyancy number and the partition coefficient on the evolution of the
 397 concentrations in salts of the ocean and the HP ice layer over time. When B_{salts} is 0, the salts have no impact on the

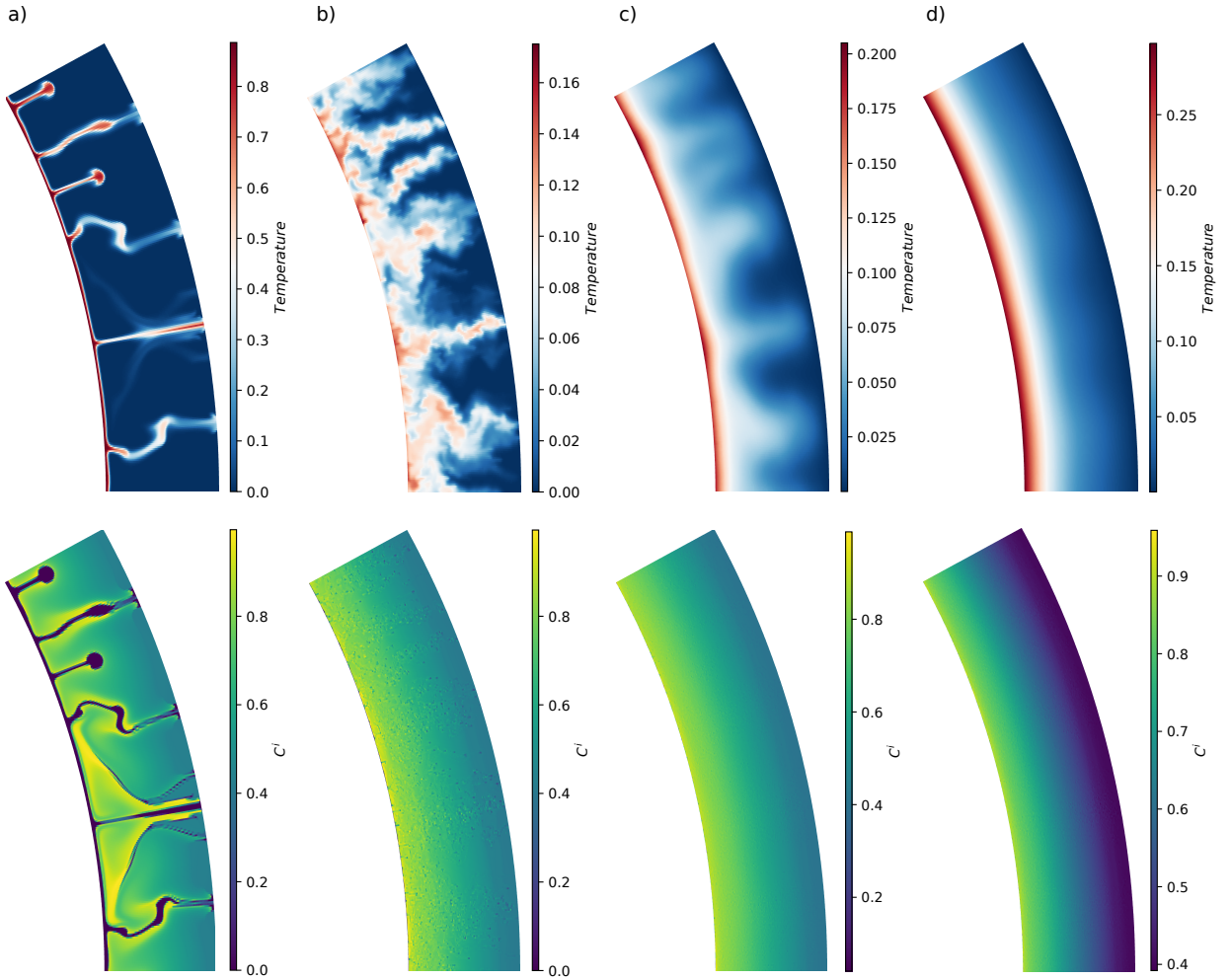


Figure 5: Snapshots of the evolution in time of 1/12 of the HP ice layer for a Rayleigh number $Ra_q = 10^7$, a radius ratio $\gamma = 0.8$, a partition coefficient $K = 1$ and a buoyancy number $B_{salts} = 10$. The top (resp. bottom) panels show the temperature (resp. composition) inside the ice shell for a) $t = 10^{-5}$, b) $t = 4.5 \times 10^{-4}$, c) $t = 7.5 \times 10^{-3}$ and d) $t = 4 \times 10^{-2}$. Note that colorbars differ between panels.

398 ice density and the salts/ice mixture has the same density as pure ice. In that case, the salts are transported passively
 399 through the HP ice layer until they reach the ocean. This is what happens in Fig. 6.a, the concentration of salts in the
 400 ocean is increasing steadily with time as the salts are easily transported by thermal convection from the core to the
 401 ocean. On the other hand, the higher the buoyancy number, the higher the density of the salts/ice mixture compared
 402 to pure ice. As can be seen in Fig. 6.d for $B_{salts} = 10$, the concentration of salts in the HP ice layer is continuously
 403 increasing because the salts mostly accumulate at the bottom of the HP ice layer, thus the density of the HP ice and
 404 salts mixture increases with time. However, a part of this mixture still rises through the ice and reaches the ocean. At
 405 the beginning of the simulation, the concentration of salts in the ice is small enough to allow a part of the salts/ice
 406 mixture to rise efficiently through the ice and the ocean concentration of salts increases rather strongly (fig. 6.b). After
 407 a certain amount of time, the proportion of salts becomes higher in the ice shell, less salts are reaching the ocean and
 408 the rate of increase of ocean salt concentration stabilizes to a smaller value (fig. 6.b).

409 The partition coefficient of the salts between the ocean and the HP ices at the top interface controls the amount
 410 of salts trapped in the ice when a part of the ocean freezes at the top interface. When $K = 0$, salts are not trapped in
 411 the ice during the re-crystallisation of the liquid water and, as can be seen in Fig. 7.c, after a certain amount of time,

Table 2Time $t^{1/2}$ required to evolve halfway to the steady-state concentration.

K	B_{salts}	$t^{1/2}$
1	0	2×10^{-5}
	0.1	1.5×10^{-5}
	0.5	9×10^{-6}
	1	6×10^{-6}
	3	3×10^{-6}
	10	10^{-6}
0.001	0	2×10^{-5}
	0.1	
	0.5	
	1	
	3	
	10	

412 the concentration of salts in the HP ice layer reaches a compositional steady state. Indeed, as $B_{salts} = 0$ and $K = 0$,
 413 after the onset of convection, the amount of salts entering the HP ice layer from the core is similar to that entering the
 414 ocean at each time step, which leads to this quasi-steady state. On the other hand, the higher the partition coefficient,
 415 the higher the amount of salts trapped during the re-crystallisation at the interface. In the case $B_{salts} = 0$ and $K = 1$,
 416 the concentration of salts in the HP ice layer continues to increase over time, as well as the concentration of salts in
 417 the ocean, as shown in Fig. 7.b and Fig. 7.d.

418 All the runs have been performed for an efficient phase change at top, with a phase change number $\Phi = 10^{-2}$. For
 419 this reason, whatever the buoyancy number and the partition coefficient, the ice in the ascending hot plumes that reaches
 420 the ocean melts at its contact, the boundary is permeable and the radial velocity at the top is much higher than 1. The
 421 convection pattern is the same for all cases shown in Fig. 8, composed of upwelling hot plumes and downwelling cold
 422 and broad currents. For the case $B_{salts} = 10$, the salts significantly increase the salts/ice mixture density. Therefore,
 423 they accumulate just above the interface between the core and the ice, as can be seen on the compositional field of
 424 Fig. 8.c, which increases the bottom temperature (See 3.2.3) and leads to an ocean very poor in salts as shown on
 425 Fig.6.b. In contrast, in Fig. 8.a and 8.b for $B_{salts} = 0$, the salts follow the heat convection pattern, as the salts have no
 426 or a low effect on the ice density for low values of the buoyancy number. Also, the ice is on average richer in salts in
 427 Fig. 8.a due to the higher partition coefficient.

428 3.2.2. Compositional flux accuracy

429 To check the accuracy of the numerical treatment of the flux of salts we impose at the interface between the core
 430 and the HP ice layer, defined in 2.2.2 and set to $F_{salts} = 1$ in the second series of runs (#2 in Table 1), we compute the
 431 total rate of increase of the salt concentration in both layers and divide it by the surface of the lower interface between
 432 the ice and the core, which should be equal to the target flux coming from the core:

$$F_{salts}^{eff} = \frac{\Delta C^i V^i + \Delta C^o V^o}{4\pi r^{-2} \Delta t}, \quad (27)$$

433 with ΔC^i (resp. ΔC^o) the variation of the salt concentration in the ice (resp. ocean) over Δt . The numerical accuracy
 434 analysis is available in appendix 6.

435 3.2.3. Time evolution

436 Let us now turn to a systematic exploration of the effect of the various control parameters. Figure 9 shows the
 437 rate of change of the concentration in salts of the ocean dC^o/dt and the HP ice layer dC^i/dt as function of the salts
 438 buoyancy number and for various values of the partition coefficient K . These rates are computed over a time period
 439 chosen after the stabilization of the concentration slope in the two layers (See § 3.2.1), here between $t_1 = 10^{-2}$ and the

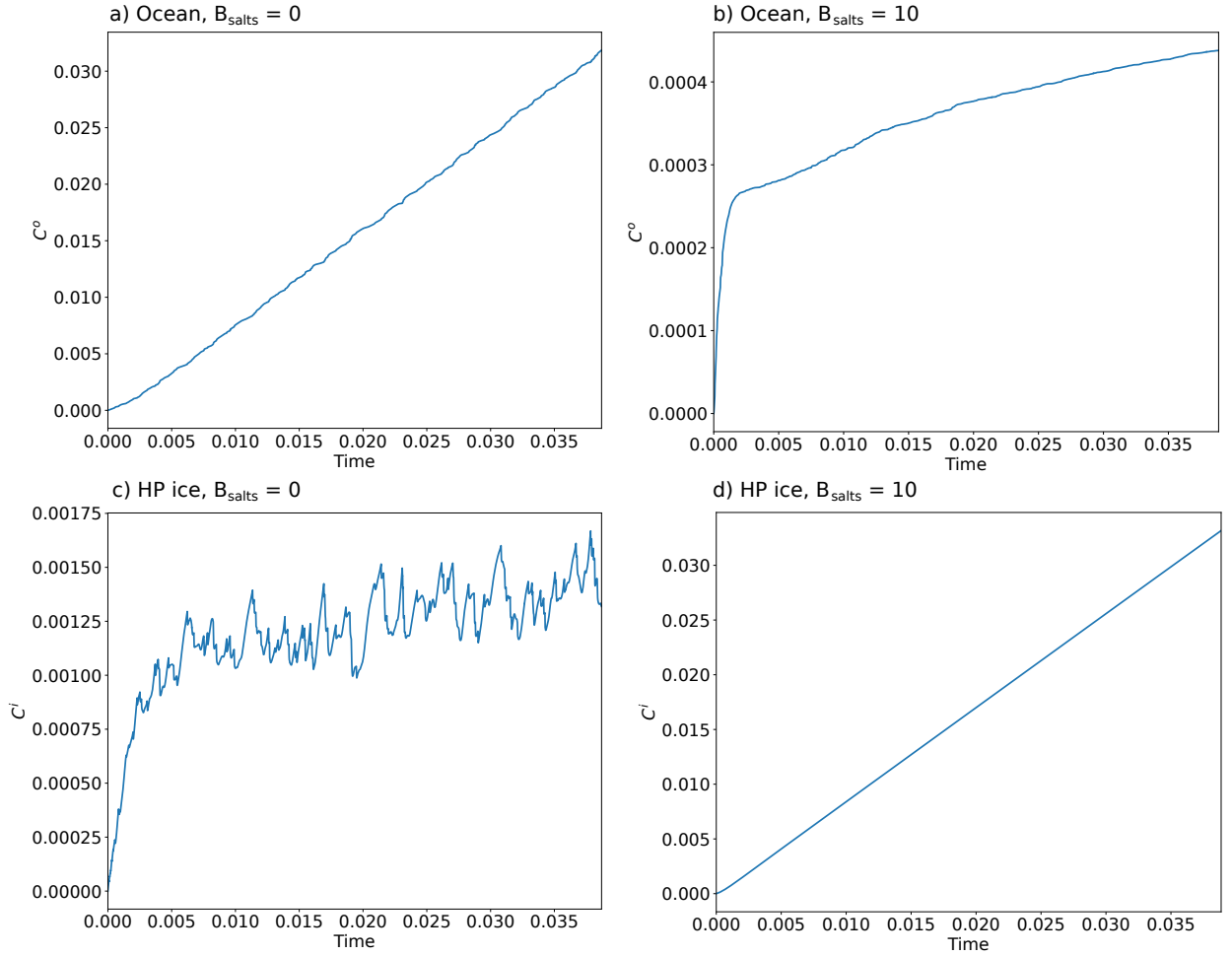


Figure 6: Evolution of the ocean a)&b) and HP ice layer c)&d) average concentrations of salts as function of time for a buoyancy number a)&c) $B_{salts} = 0$ and b)&d) $B_{salts} = 10$. Both a)&c) and b)&d) are for a Rayleigh number of 10^8 , a partition coefficient of the salts between the ocean and the HP ices at the top interface of $K = 10^{-2}$ and a radius ratio of $\gamma = 0.9$.

440 end of the runs $t_2 = 3.8 \times 10^{-2}$. Due to the conservation of salts, the expression of the mass balance is:

$$\frac{(dC^o/dt)V^o + (dC^i/dt)V^i}{V^o + V^i} = \frac{4\pi(r^-)^2 F_{salts}^{eff}}{V^o + V^i}, \quad (28)$$

441 and we note S_C the average rate of increase in solid and liquid concentration:

$$S_C = \frac{4\pi(r^-)^2 F_{salts}^{eff}}{V^o + V^i}. \quad (29)$$

442 Since the salt flux at the bottom of the ice layer is equal to one by our choice of scaling, the value of this sum is purely
 443 geometrical and, for the same ocean radius R_o , depends only on the radius ratio, which defines the thickness of the HP
 444 ice layer and, consequently, that of the ocean. The thickness of the HP ice (resp. ocean) layer increases (resp. decreases)
 445 for decreasing values of the radius ratio (there is a factor 2.25 on the thickness d between $\gamma = 0.8$ and $\gamma = 0.9$). For the
 446 ocean radius defined in § 2.2.1 corresponding to a Ganymede-like case, the theoretical value of S_C is about 0.43 for
 447 $\gamma = 0.8$ and about 0.22 for $\gamma = 0.9$ (See grey line on Fig. 9.a and Fig. 9.b). As shown on Fig. 9, for low values of the

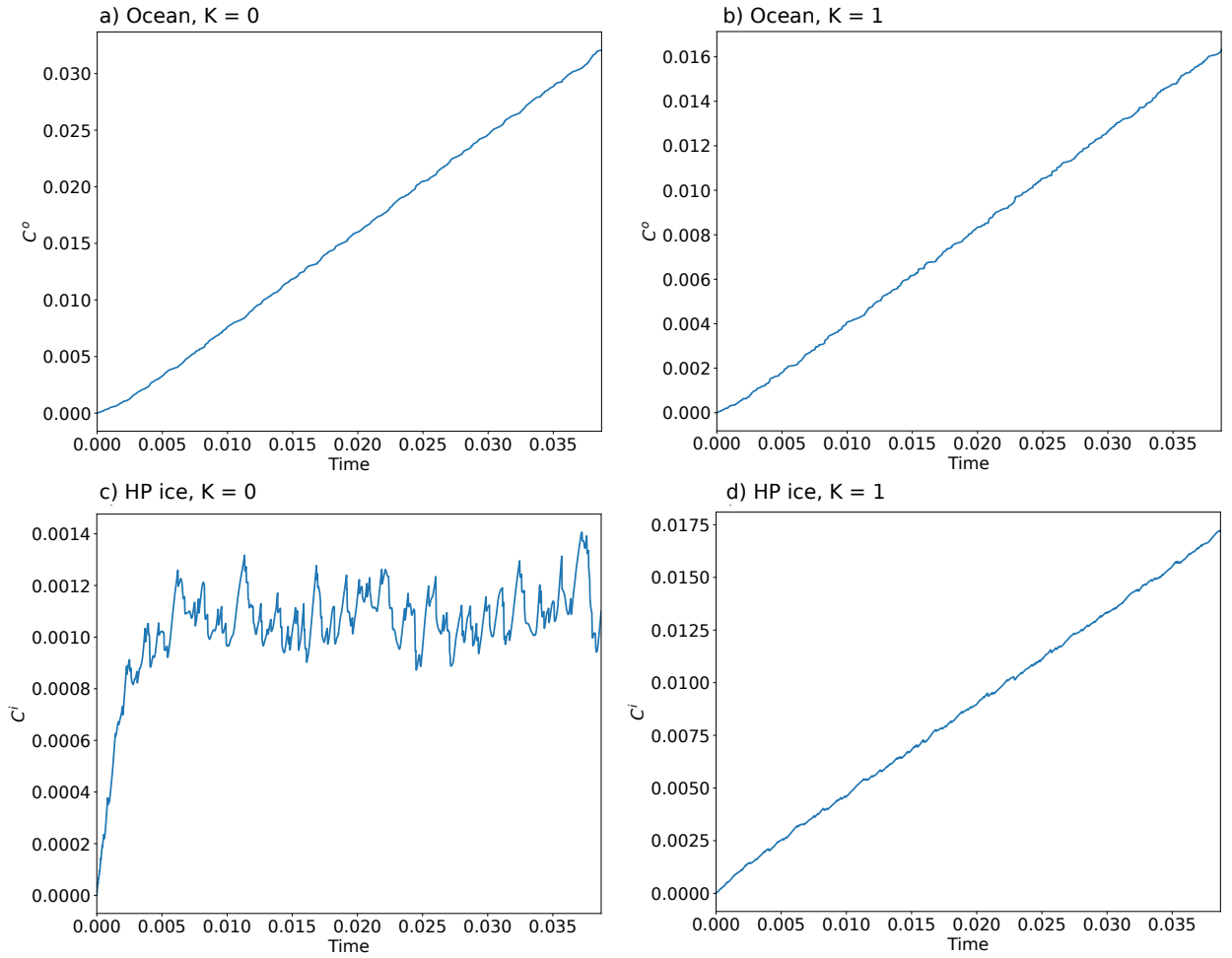


Figure 7: Evolution of the ocean a)&b) and HP ice layer c)&d) average concentrations of salts as function of time for a partition coefficient of the salts between the ocean and the HP ices at the top interface of a)&c) $K = 0$ and b)&d) $K = 1$. Both a)&c) and b)&d) are for a Rayleigh number of 10^8 , a buoyancy number of $B_{salts} = 0$ and a radius ratio of $\gamma = 0.9$.

448 buoyancy number ($B_{salts} \leq 0.6$ for $\gamma = 0.8$ and $B_{salts} \leq 0.5$ for $\gamma = 0.9$), the value of both rates of change (ocean and
 449 ice) equals the value of S_C for $K = 1$. From eq. 28, we can compute the two extreme cases for which the rate of change
 450 in the ice dC^i/dt or in the ocean dC^o/dt is 0, meaning that all the salts are transported to the other layer, which gives
 451 us its maximum rate of change. These maximum values, around $0.86 - 0.87$ for both layers for $\gamma = 0.8$ (because both
 452 volumes are similar in that case) and about 0.29 in the ocean and 0.97 in the ice for $\gamma = 0.9$, are represented on Fig. 9
 453 by a red dotted line for the ocean and an orange dashed line for the ice. As can be expected, dC^i/dt tends towards its
 454 maximum value for increasing values of the buoyancy number, which for all values of K is reached for $B_{salts} \gtrsim 1$.
 455 On the other hand, dC^o/dt tends towards its maximum value for decreasing values of the buoyancy number and low
 456 values of K , that is for $K \lesssim 0.1$ and $B_{salts} \lesssim 0.5$.

457 According to Fig. 9, the proportion of salts in the ocean compared to the proportion in the ice shell reverses at a
 458 certain buoyancy number, which is the limit between the low buoyancy number regime and the high buoyancy number
 459 regime. For $Ra_q = 10^8$ this limit is around $B_{salts} = 0.6$ for $\gamma = 0.8$ (see Fig. 9.a) and between $B_{salts} = 0.5$ and 0.6 for
 460 $\gamma = 0.9$ (see Fig. 9.b). For each partition coefficient, the closer the buoyancy number is to this limit value, the closer
 461 dC^o/dt and dC^i/dt become. For B_{salts} ranging from ~ 1 to 10 , dC^i/dt is close to the maximum value identified with
 462 eq. 29, leading to a similar concentration in salts in the ice at the end of the runs in all three cases presented here. The
 463 rate of change of the concentration in the ocean dC^o/dt in those cases is $< 10^{-1}$. This is consistent with the fact that

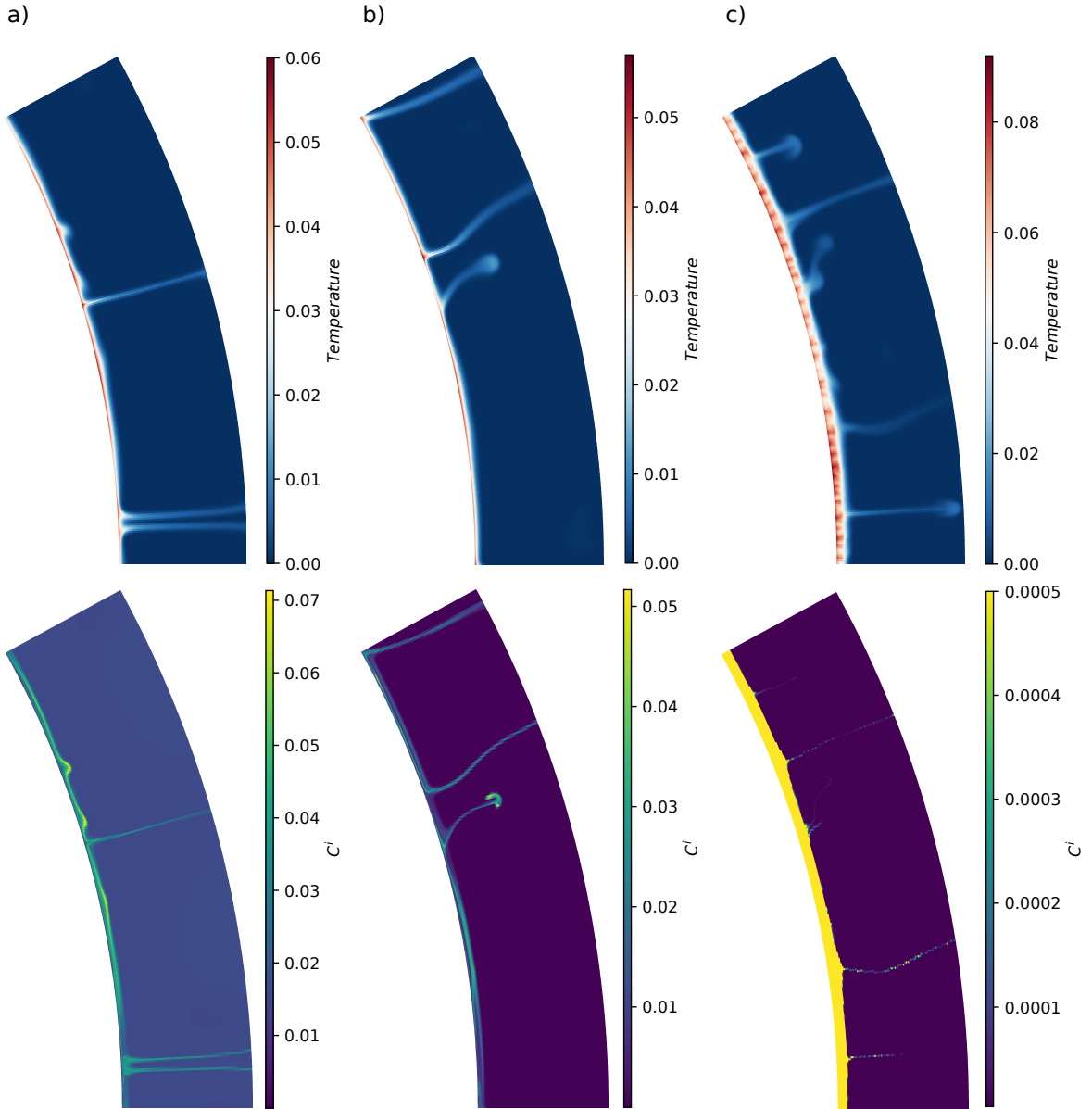


Figure 8: Snapshots of $1/12$ of the HP ice layer after stabilization of the slopes of concentration increase in the ocean and in the ice over time at $t \simeq 4 \times 10^{-2}$ for a Rayleigh number $Ra_q = 10^8$, a radius ratio $\gamma = 0.8$. The top (resp. bottom) panels show the temperature (resp. composition) inside the ice shell for a) $K = 1$ and $B_{salts} = 0$, b) $K = 10^{-2}$ and $B_{salts} = 0$, c) $K = 10^{-2}$ and $B_{salts} = 10$. The maximum concentration of salts in the HP ice layer for c) is about 0.57 but the color bars have been limited to 5×10^{-4} in order to have more information about what happens in the bulk of the ice shell. Note that colorbars differ between panels.

464 the salts accumulate at the bottom of the ice shell, preventing an efficient transfer of salts toward the ocean. For low
 465 values of the buoyancy number, $B_{salts} < 0.6$, the salts have a very low impact on the ice density and are transported
 466 easily by convection in the solid state through the HP ice layer. In those cases, the range covered by dC^i/dt as function
 467 of B_{salts} is very large, because almost the entire amount of salts coming from the core are transported into the ocean
 468 and the evolution of the salts concentration in the ice shell depends mostly on the amount of salts trapped into the ice
 469 when a part of the ocean at the interface with the HP ices refreezes and is accreted to the ice, which is controlled by
 470 K . In Fig. 9, this is reflected in the fact that dC^i/dt decreases with decreasing values of the partition coefficient, while

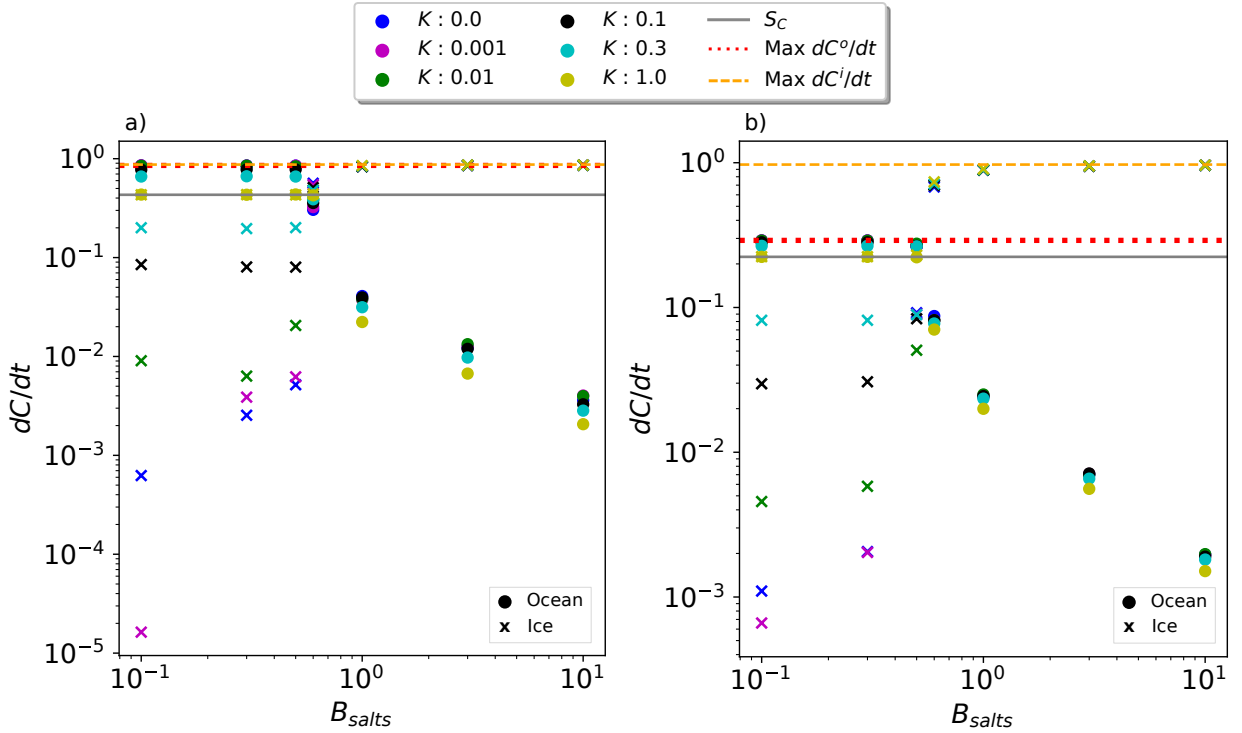


Figure 9: Rate of change of the concentration in salts of the ocean (\bullet) and of the HP ice layer (\times) over time as function of the salts buoyancy number for a radius ratio a) $\gamma = 0.8$ and b) $\gamma = 0.9$. This has been computed for various values of K , for a Rayleigh number of $Ra_q = 10^8$ and a zero initial concentration C_{ini} in the ocean and in the HP ice layer. The grey line is the result of eq.29 and the two other lines are the maximum rate of change that can be reached in the ocean (red dotted line) and in the ice (orange dashed line).

471 it is exactly equal to dC^o/dt for $K = 1$, for which the amount of salts trapped into the ice at the interface is maximal.
 472 In Fig. 9.a and b, for $B_{salts} = 10^{-1}$, dC^i/dt for $K = 0$ and $K = 10^{-3}$ are swapped compared to what we could expect.
 473 Indeed, the values of dC^i/dt are really low and fall within the error bar computed in appendix 6. The values of dC/dt
 474 also tend to get mixed up for $B_{salts} \sim 0.5$, which corresponds to the transition between a well mixed ice layer and a
 475 stratified one. In this transitional region of the parameter space, fluctuations are important and make the determination
 476 of dC/dt subject to more uncertainty than in the two end-member regimes. For the concentration of salts in the ice,
 477 the value of K has nearly no effect for $B_{salts} \gtrsim 1$ but a significant effect for $B_{salts} < 0.6$.

478 While the ocean is considered homogeneous by construction of the model, the salts concentration is not uniform
 479 in the HP ice layer and their distribution in the shell is controlled by the values of the partition coefficient and the
 480 buoyancy number. Figure 10 shows the profiles of temperature (left panels) and composition (right panels) in the HP
 481 ice layer for a partition coefficient of 1 and various values of the buoyancy number at different times of the runs.
 482 These times are similar between the three presented cases, $B_{salts} = 0$, $B_{salts} = 0.7$ and $B_{salts} = 10$ in order to make
 483 the comparisons relevant. For a buoyancy number $B_{salts} = 0$ the salts have no effect on the density. Therefore, the
 484 temperature curves through the ice shell (fig. 10.a) have a classical shape for the boundary conditions of the problem,
 485 with $\tilde{T}^+ = 0$ as set in equation 21 and a thermal boundary layer at the bottom, which does not thicken in time. In terms
 486 of composition (fig. 10.b), the concentration of salts is slightly higher around the height at which they are added to the
 487 ice shell (see § 2.2.2) but the overall layer is poor in salts because they are easily transported by convection as they
 488 have no impact on density in that case. Due to the value of the partition coefficient, $K = 1$, the concentration of salts
 489 in the bulk increases as fast as in the ocean with time. For $B_{salts} = 0.7$, a buoyancy number just above the limit value
 490 for $Ra_q = 10^8$ and $\gamma = 0.8$ (see Fig.9), the temperature profile evolves a lot more with time (fig. 10.c). At the onset of
 491 convection and until $t \sim 1.69 \times 10^{-2}$, there is a classical thermal boundary layer at the bottom, which thickens with

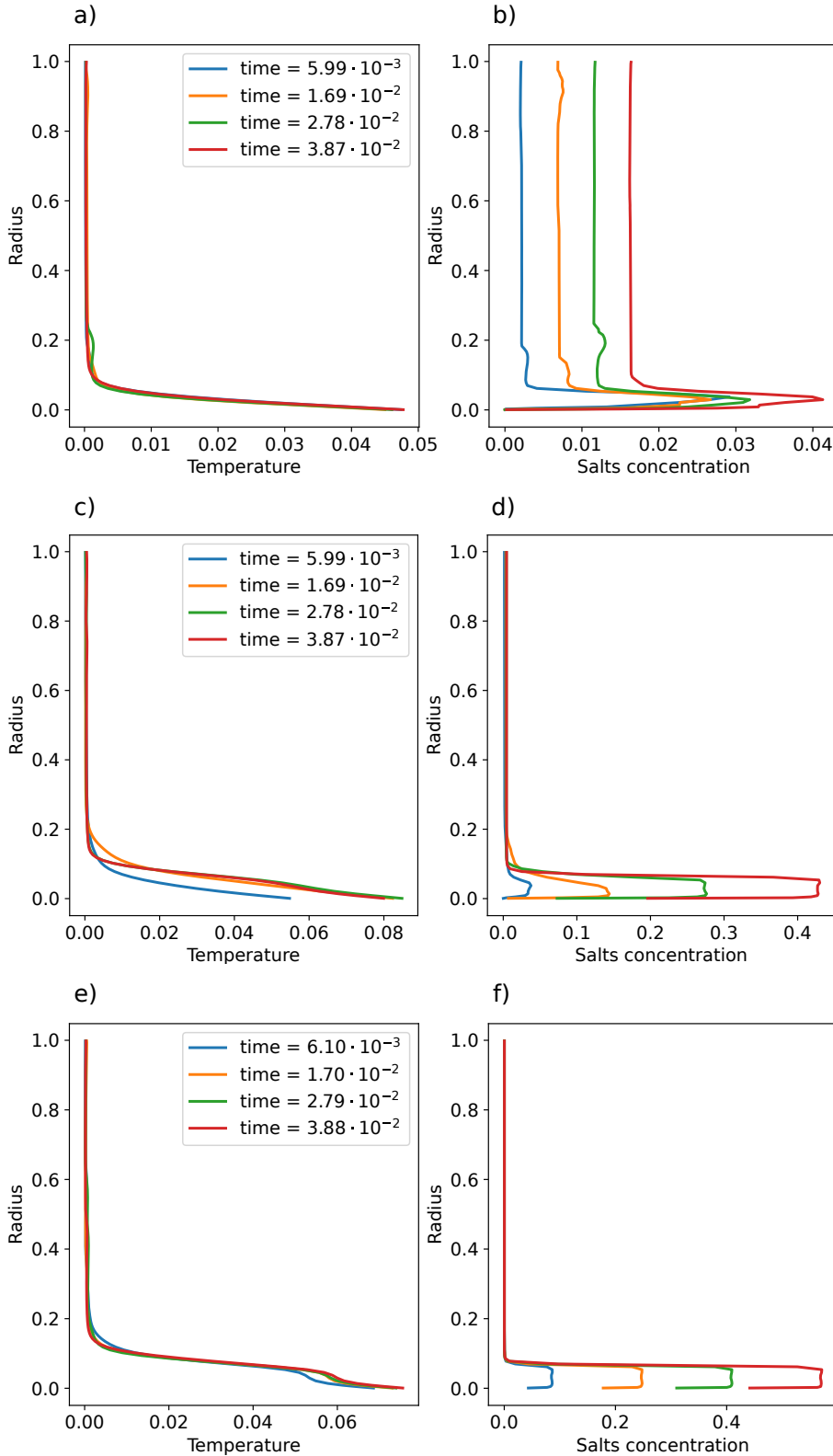


Figure 10: Profiles of the temperature and the salts concentration in the HP ice layer as function of the radius at different times of the simulation. This figure is for a partition coefficient $K = 1$, a Rayleigh number $Ra_q = 10^8$ and a radius ratio $\gamma = 0.8$. Panels a) & b) are for $B_{salts} = 0$, c) & d) for $B_{salts} = 0.7$ and e) & f) for $B_{salts} = 10$.

492 time. Around this time, a layering seems to happen and there are two separate thermal boundary layers. In that case,
 493 a salts-rich layer develops at the bottom of the ice shell and it thickens with time (fig. 10.d). Finally, for a very high
 494 buoyancy number $B_{salts} = 10$, there is already a layering of the convection and two thermal boundary layers at the
 495 bottom early in the simulation. Also, the mixture of salts and ice that forms the lower, highly salted layer is so dense
 496 that the salts can hardly be carried by convection to the upper layer, which thus remains lighter than this salts-rich
 497 lower layer.
 498

3.2.4. Salts transport

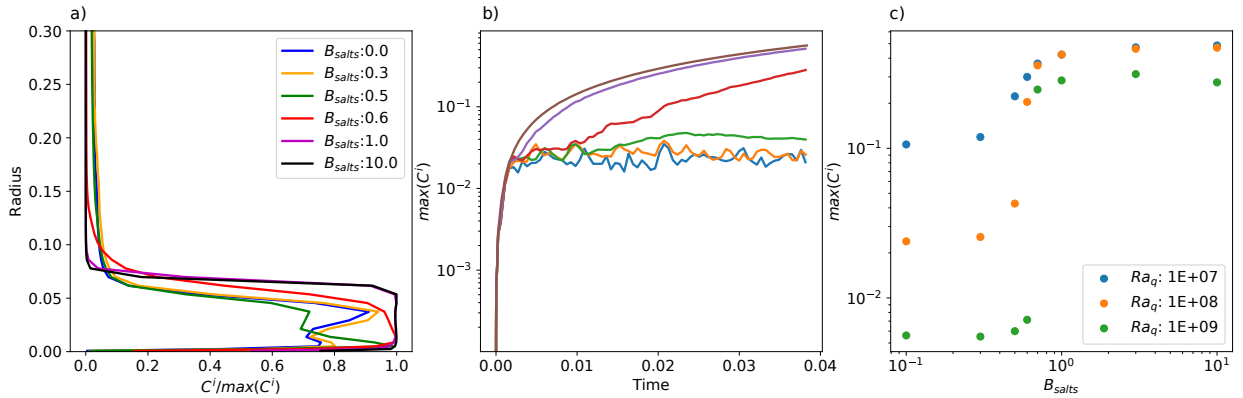


Figure 11: a) Profile of the concentration in salts at the bottom of the HP ice layer divided by the maximum concentration $\max(C^i)$ as function of the radius for various values of the buoyancy number. b) Maximum concentration in salts of the HP ice layer $\max(C^i)$ as function of time. c) Maximum concentration in salts of the HP ice layer $\max(C^i)$ for various values of the Rayleigh number as function of B_{salts} . This figure is for a partition coefficient $K = 10^{-2}$ and a radius ratio $\gamma = 0.8$. a) and b) are for a Rayleigh number $Ra_q = 10^8$. a) and c) are time-averaged over a period between $t_1 = 2.6 \times 10^{-2}$, chosen after the stabilization of the concentration slopes (See § 3.2.1) in the ocean and in the ice, and $t_2 \simeq 3.9 \times 10^{-2}$ the end of the simulation.

500 In this part, we study the effect of the buoyancy number on the salts distribution through the HP ice layer (fig. 11.a)
 501 and the evolution of the maximum concentration in salts with time (fig. 11.b) and as function of B_{salts} (fig. 11.c). We
 502 also analyze the temperature, radial velocity, thermal and compositional advection profiles for low (fig. 12) and high
 503 (fig. 13) values of the buoyancy number separately. The thermal advection reflects how heat is transferred through the
 504 shell and can be written from eq. 5 as $w\Delta\tilde{T}$. The compositional advection reflects how the salts are transported by
 505 convection and can be written from eq. 6 as $w\Delta C^i$. We chose a time period after the stabilization of the concentration
 506 slope in the ocean and in the ice (See § 3.2.1), here from $t_1 = 2.6 \times 10^{-2}$ to the end of the simulation $t_2 = 3.9 \times 10^{-2}$. The
 507 panels a) and c) of Fig. 11 and all profiles of Figures 12 and 13 are time-averaged on this period. This period is long
 508 enough for these parameters to evolve a lot, in particular the concentration of salts and the temperature. Therefore,
 509 these two curves are built by dividing the relevant parameter by a reference value: the bottom temperature \tilde{T}^- for
 510 Figures 12.a and 13.a and the maximum concentration $\max(C^i)$ for Fig. 11.a, before averaging over time. Figure 11.b
 511 shows the evolution of the maximum concentration as function of time for $Ra_q = 10^8$ and various values of the
 512 buoyancy number, while Fig. 11.c shows the time-averaged value of the maximum value as function of the buoyancy
 513 number for various Rayleigh numbers.

514 It is clear in all panels of Fig. 11 that there is a very marked separation between two regimes: one for low values
 515 of the buoyancy number and one for high values of the buoyancy number. On Fig. 11.c, we can observe that the
 516 difference in maximum salts concentration between low and high values of the buoyancy number becomes larger with
 517 higher values of Ra_q . Also, the limit between low and high values of the buoyancy number for $Ra_q = 10^8$ is very
 518 clear in Fig. 11.c, with an inflection point between $B_{salts} = 0.5$ and $B_{salts} = 0.6$. These limit values increase with
 519 increasing Rayleigh numbers (See Fig. 11.c). These two regimes are also visible on Fig. 11.b. For low values of the
 520 buoyancy number the salts are easily transported through the HP ice layer and most of the salts coming from the core
 521 go into the ocean. As the partition coefficient is small here, $K = 10^{-2}$, the amount of salts trapped in the ice at the

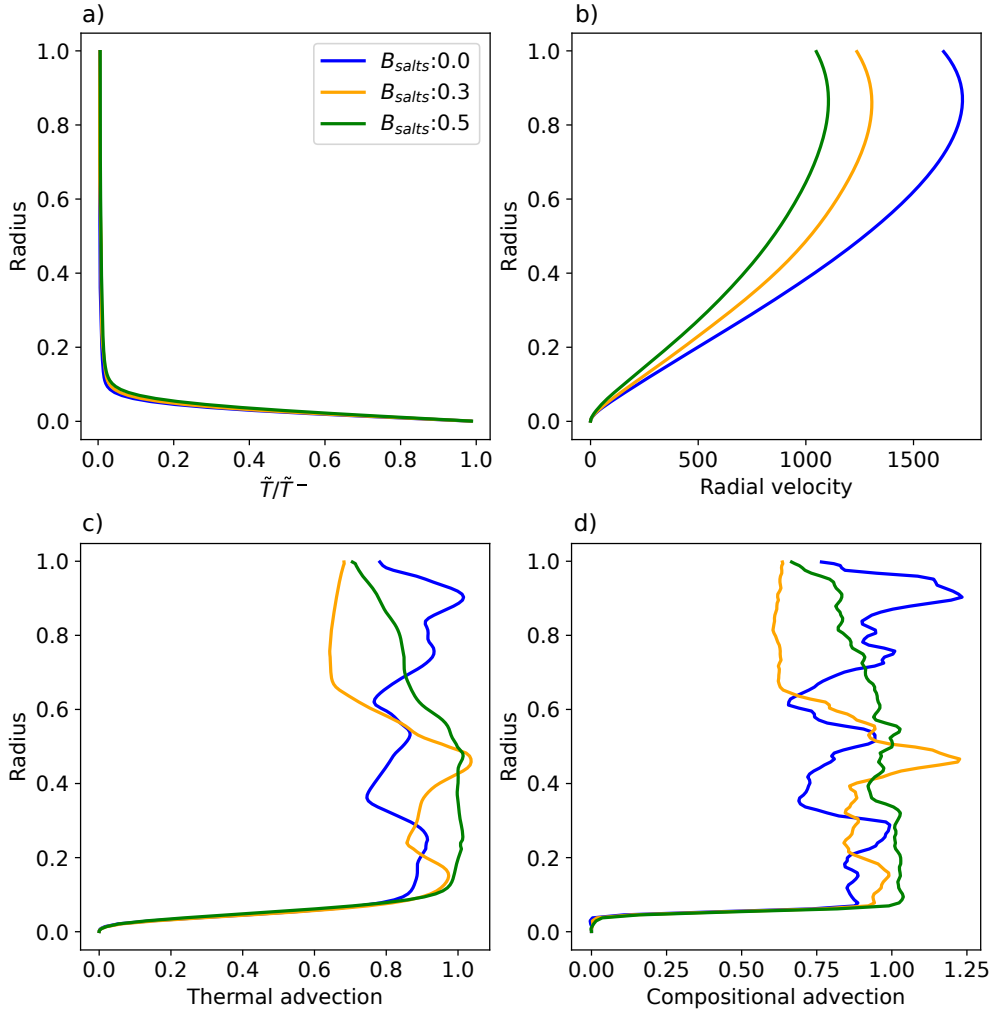


Figure 12: Profiles of a) the temperature divided by the bottom temperature, b) the radial velocity, c) the thermal advection and d) the compositional advection in the HP ice layer as function of the radius for small buoyancy number $B_{salts} \leq 0.5$. This figure is for a partition coefficient $K = 10^{-2}$, a Rayleigh number $Ra_q = 10^8$ and a radius ratio $\gamma = 0.8$. The parameters shown on the four panels are time-averaged over a period between $t_1 = 2.6 \times 10^{-2}$, chosen after the stabilization of the concentration slopes (See § 3.2.1) in the ocean and in the ice, and $t_2 \simeq 3.9 \times 10^{-2}$ the end of the simulation.

522 interface with the ocean is very low and the HP ice layer reaches a compositional steady-state. The case $B_{salts} = 0.5$ is
 523 an intermediate case, with a final maximum concentration slightly higher than that for low values of B_{salts} but it seems
 524 to also reach a compositional steady-state, unlike the cases for high values of B_{salts} . Regarding the concentration in
 525 salts divided by the maximum concentration (fig. 11.a), in the upper part of the HP ice layer it depends only weakly
 526 on B_{salts} . In this part the buoyancy number has no effect on the thermal convection because the salts concentration is
 527 small for large values of B_{salts} and does not affect the density for small values of B_{salts} and all the salts reaching this
 528 part go into the ocean. The value of the concentration in this upper part is mainly controlled by the partition coefficient
 529 K . In the lower part, two regimes can be observed, depending on the value of the buoyancy number. In the first case,
 530 for a buoyancy number $B_{salts} \leq 0.5$, the lower part is slightly enriched in salts, as can be seen on Fig. 11.a and b, due to
 531 the way the flux of salts is modeled. A concentration of salts corresponding to the desired compositional flux is directly
 532 added to the ice shell at each time step at a certain height, here $h = 0.05$ (See § 2.2.2), which corresponds more or less
 533 to the maximum of the concentration in this salt-poor layer. In the regime for high values of the buoyancy number,
 534 $B_{salts} > 0.5$, the density of the salts/ice mixture is so much larger than that of pure ice that the salts accumulate at the
 535 bottom of the HP ice layer. It creates a highly salted layer (See Fig. 11.a and Fig. 11.b) thicker than in the cases with

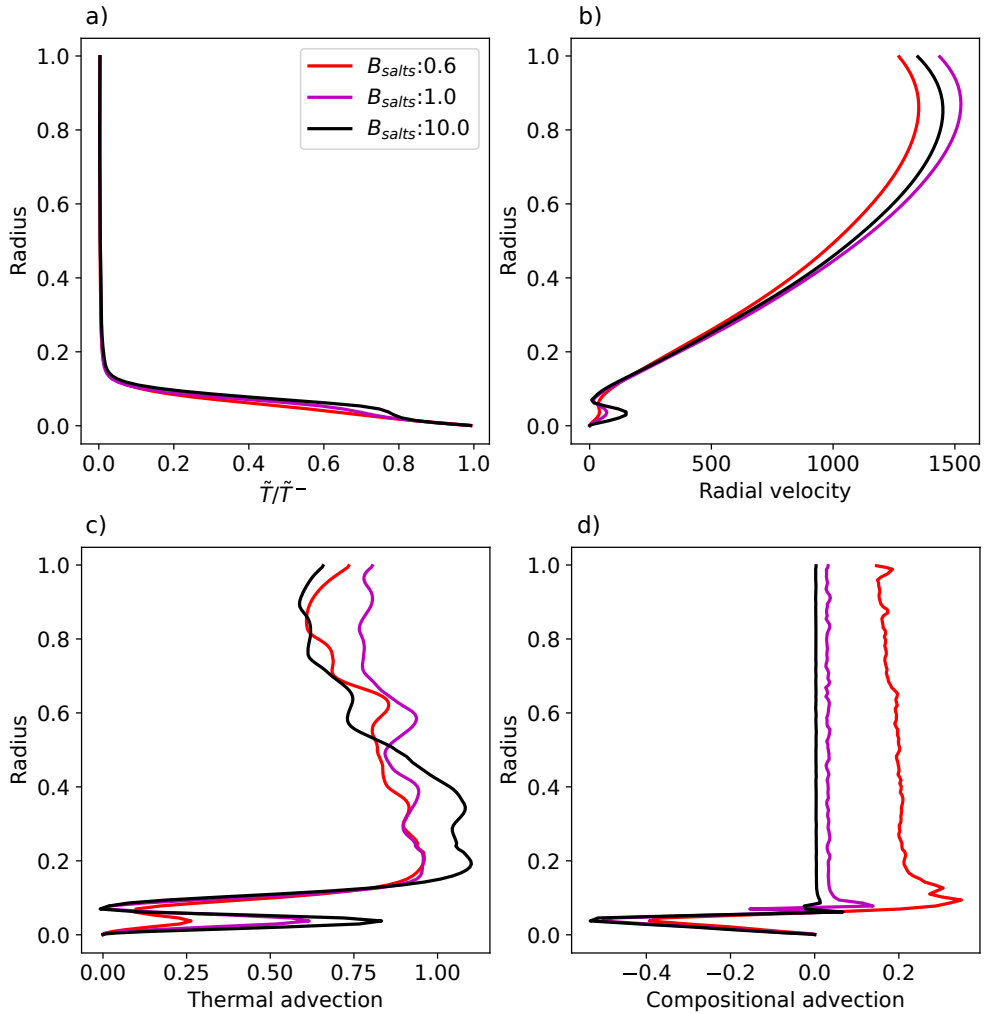


Figure 13: The same as in Fig. 12 but for $B_{salts} > 0.5$.

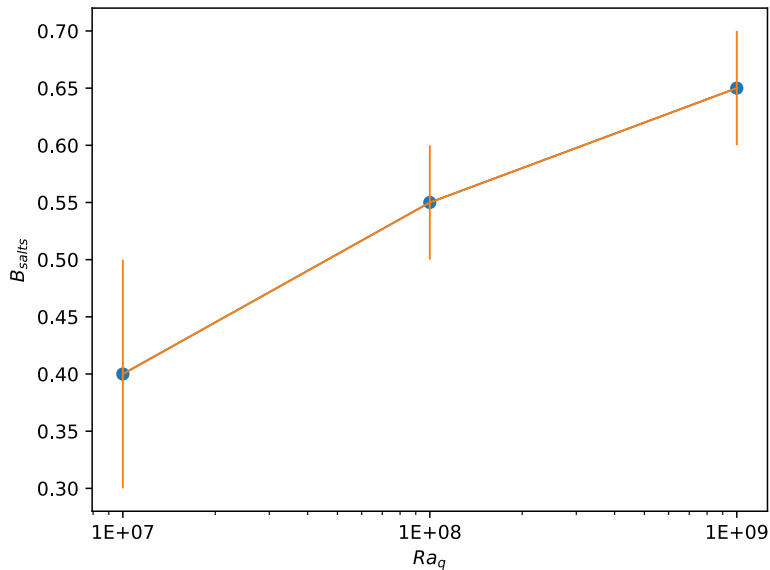
536 a low buoyancy number. This thickening is probably due to a modest entrainment by the thermal convection above
 537 which transports a small part of the salts to the top and leaves the rest at the bottom.

538 In Fig. 12, for low values of the buoyancy number, the shape of the different curves corresponds to what we could
 539 expect with pure ice (Lebec et al., 2023). In Fig. 12.a there is a classical thermal boundary layer at the bottom of the
 540 shell and a temperature of almost 0 in the rest of the layer due to the temperature boundary conditions (See § 2.1.2).
 541 Also, the thermal boundary layer does not change significantly with variable values of B_{salts} . In this regime, the
 542 thermal advection curves plotted in Fig. 12.c increase with radius in the thermal boundary layer until reaching a value
 543 of around ~ 1 in the rest of the shell, which is the value needed to balance the imposed flux at the bottom boundary.
 544 The compositional advection (fig. 12.d), on the other hand, is just slightly negative under the part where the salts are
 545 added to the HP ice layer and increases in the rest of the thermal boundary layer until reaching ~ 1 , which is also the
 546 value of the imposed influx at the bottom. Concerning the radial velocity (fig. 12.b), the inflection at the bottom is due
 547 to the rigid boundary condition and in the rest of the shell it decreases for increasing values of B_{salts} .

548 For the high buoyancy number regime, the same parameters are displayed in Fig. 13. In those cases, in Fig. 13.a,
 549 there is an inflection point of temperature at a radius grossly set by the position at which salts are introduced in the
 550 shell (See 2.2.2) and there are two thermal boundary layers, which is a sign of layering of the convection (It can be
 551 observed on Fig. 8). A few tests varying the position of salts introduction (not shown) have confirmed that it sets
 552 the thickness of the bottom layer. Beside this, this choice has no effect on the dynamics. The inflection gets more

553 pronounced for increasing values of the buoyancy number B_{salts} . The thermal advection (fig. 13.c), increases with
 554 height classically along the first thermal boundary layer at the bottom, then decreases until reaching a local minimum
 555 between the two convective layers before increasing again along a second thermal boundary layer. The compositional
 556 advection (fig. 13.d), is negative at the bottom of the HP ice layer, implying that the salts are transported downwards,
 557 which is consistent with a layering of the convection. The compositional advection is low in the rest of the HP ice layer
 558 due to the fact that most of the salts remain at the bottom of the shell. The point where the thermal and compositional
 559 advection profiles reach their local minima is the interface between the two distinct convective layers. The thickness of
 560 the lower convective layer is essentially set by the height at which the salts are added, which is somewhat arbitrary in
 561 the model. Therefore, the exact value of the thickness of this layer is not relevant, but we think this effect would occur
 562 naturally because of the way the salts/water mixture should rise through the ice before recrystallizing (See Fig. 1.b).
 563 This layering of the convection is also affecting the radial velocity profile (fig. 13.b), which shows a local maximum
 564 in the middle of the lower layer while the upper layer has a shape similar to that obtained for the whole ice layer in the
 565 low buoyancy number regime.

566 To summarize, two distinct dynamical regimes exist depending on the value of B_{salts} . Also, from Fig. 11.c, the
 567 critical buoyancy number for which we switch between the two regimes depends mainly on the Rayleigh number
 568 Ra_q . Therefore, we can build a regime diagram which allows us to separate the stratified convection cases from the
 569 well-mixed ones depending on B_{salts} and Ra_q , as shown on Fig. 14. Determining the exact value of B_{salts} for the
 570 regime change for a given Ra_q would require to compute solutions for a much larger number of B_{salts} values. Looking
 571 at various profiles, as shown in Fig.11.a, Fig. 12 and Fig. 13, allows us to bracket the transition value of B_{salts} . For
 572 each value of Ra_q available in this study, this method gives us an interval for B_{salts} over which the transition occurs
 and Fig. 14 shows the medians of each interval as points and the lengths as error bars.



573
 574 **Figure 14:** Regime diagram showing the separation between well-mixed and stratified convection regimes depending on
 the buoyancy number B_{salts} and the Rayleigh number Ra_q .

573

574 3.3. Scaling laws

575 Several scaling laws can be proposed in order to quantify the effect of salts on the mass transfer efficiency through a
 576 HP ice layer, such as the root-mean-square (RMS) radial velocity at the top interface with the ocean and the temperature
 577 at the bottom interface with the core as function of the Rayleigh number, and the ratio of outflow to the ocean and inflow
 578 from the core as function of the buoyancy number.

Table 3

Values of the scaling coefficients for the laws $w_{top} = c_w Ra_q^{p_w}$ and $Nu = c_T Ra_q^{p_T}$ for $\gamma = 0.8$ and $\gamma = 0.9$, with $K = 10^{-2}$

B_{salts}	$\gamma = 0.8$				$\gamma = 0.9$			
	w_{top}		Nu		w_{top}		Nu	
	c_w	p_w	c_T	p_T	c_w	p_w	c_T	p_T
0.0	0.13	0.51	0.25	0.24	0.18	0.5	0.3	0.23
0.1	0.17	0.49	0.22	0.25	0.15	0.51	0.25	0.24
0.3	0.1	0.52	0.15	0.27	0.14	0.5	0.21	0.25
0.5	0.22	0.46	0.04	0.33	0.36	0.44	0.03	0.35
1	0.1	0.52	0.14	0.25	0.17	0.49	0.22	0.22
3	0.19	0.49	0.21	0.22	0.19	0.49	0.29	0.2
10	0.14	0.5	0.17	0.24	0.18	0.49	0.3	0.2

579 Both the radial velocity at the top and the bottom temperature are important output parameters to quantify the
 580 efficiency of the heat and mass transfer through the HP ice layer. A higher radial velocity at the interface with the
 581 ocean means more efficient mass transfer through the boundary, while the bottom temperature is directly related to
 582 the amount of melt at the interface between the core and the HP ice shell. According to Lebec et al. (2023), a relation
 583 exists between the radial velocity and the Rayleigh number $w_{top} = c_w Ra_q^{p_w}$ and also between the Nusselt number Nu ,
 584 the dimensionless heat flux, and the Rayleigh number $Nu = c_T Ra_q^{p_T}$, with c_w, p_w and c_T, p_T the scaling coefficients for
 585 these two laws. In our case of a fixed heat flux, the Nusselt number is defined as $Nu = 1/\Delta\tilde{T}$, with $\Delta\tilde{T} = \tilde{T}^+ - \tilde{T}^-$ the
 586 mean dimensionless temperature difference between the upper and the lower boundaries, which allows us to compute
 587 the dimensional horizontal average bottom temperature T^- . For the case without salts (Lebec et al., 2023), we obtained
 588 the following scaling exponents: $p_w = 1/2$ and $p_T = 1/5$.

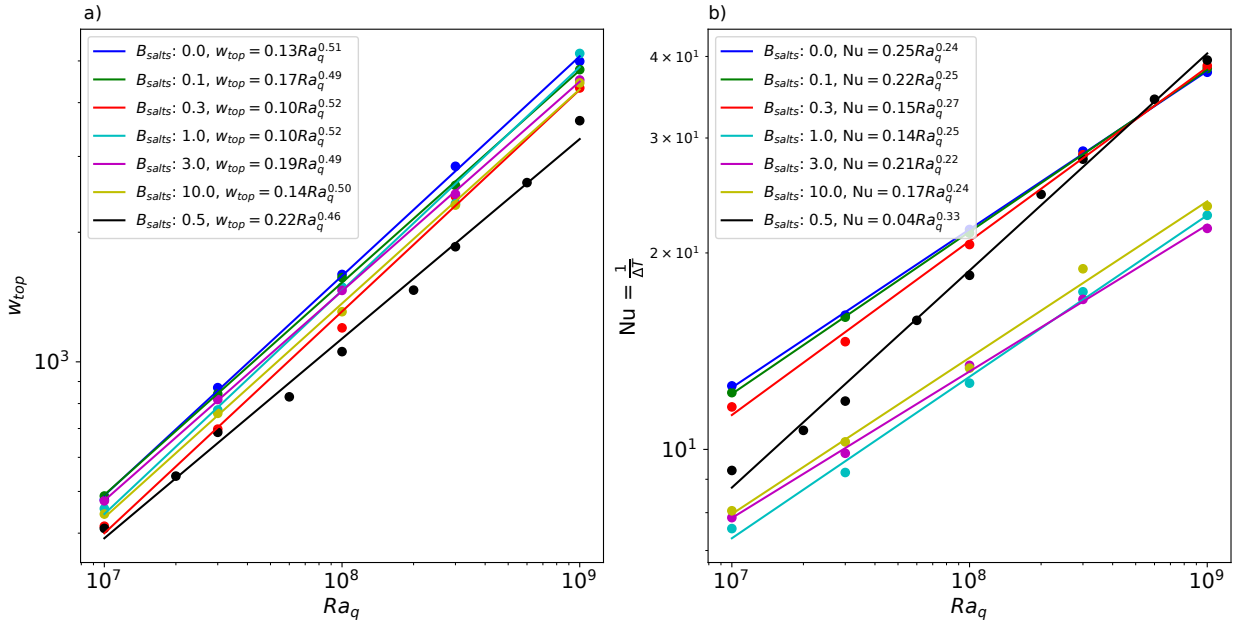


Figure 15: a) Dimensionless radial velocity at the top boundary of the HP ice layer and b) Nusselt number, $Nu = \frac{1}{\Delta T}$ with ΔT the dimensionless temperature through the ice shell, as functions of the Rayleigh number for various values of B_{salts} , a radius ratio $\gamma = 0.8$ and a partition coefficient of salts between the ice and the ocean fixed to $K = 10^{-2}$.

589 These two relations have been plotted in Fig. 15 for $K = 10^{-2}$, $\gamma = 0.8$ and various values of the buoyancy number
 590 and there are several important points to note. First of all, the scaling exponents are in the range $p_w = 0.49 - 0.52$

591 for w_{top} , which is about $1/2$, and $p_T = 0.22 - 0.27$ for Nu , which is about $1/4$. The exponent for the Nusselt number
 592 is slightly higher than the one obtained in Lebec et al. (2023) for a radius ratio of $\gamma = 0.95$. The scaling coefficient
 593 p_T presented in Table 3 for a radius ratio $\gamma = 0.9$ is between $1/5$ for high values of the buoyancy number, which
 594 corresponds to the coefficient we obtained in Lebec et al. (2023) for the same radius ratio, and $1/4$ for low values of
 595 the buoyancy number, which corresponds to the coefficient we obtain here for $\gamma = 0.8$. This could explain the higher
 596 value obtained in Fig. 15.b for $\gamma = 0.8$. The very high power-law exponent $p_T = 0.33$ obtained for $B_{salts} = 0.5$ has been
 597 excluded from the previous ranges as it seems to be a transitional case between the low and high buoyancy numbers
 598 regimes. For a Rayleigh number $Ra_q = 10^7$, $B_{salts} = 0.5$ falls in the high buoyancy number regime, the salts have
 599 a large effect on the ice density and the Nusselt number is closer to the ones for high buoyancy numbers, while for
 600 $Ra_q = 10^9$ the salts have almost no effect on the density and the Nusselt number is closer to the values for low buoyancy
 601 numbers.

602 The addition of salts in the problem, irrespective of the value of the buoyancy number, does not seem to have a
 603 significant effect on the radial velocity at the top, at least for this range of Rayleigh numbers, meaning that the buoyancy
 604 affects the amount of salts transported via the salt/ice mixture into the ocean through the HP ice layer, but not so much
 605 the velocity at which the transfer occurs. Also, as the salts increasingly accumulate at the bottom of the HP ice layer
 606 when the buoyancy increases, one would think that the radial velocity at the top is likely to be lower for higher values
 607 of B_{salts} . This, however, is not what is observed in Fig. 15.a; instead, the lowest radial velocities are obtained for the
 608 cases $B_{salts} = 0.3$ and 0.5 . This could be due to the layering of the convection for high values of the buoyancy number.
 609 In that case, the salts accumulate in the lower convective layer and the amount of salts in the upper convective layer,
 610 closer to the surface, is low enough for the convection to remain efficient. Therefore, the radial velocity is only slightly
 611 affected, but the ice reaching the ocean is less enriched in salts. On the other hand, for $B_{salts} = 0.3$ and 0.5 , the salts
 612 are sufficient to affect the ice density and slow down the exchanges with the ocean, but this effect is too small to create
 613 a layering of the convection, which would allow, as in the previous case for high values of the buoyancy number, to
 614 maintain efficient convection in the upper layer. In this range of values, the ice reaching the ocean is more enriched in
 615 salt but the overall mass transfer across the interface is slowed by their effect on the ice density.

616 On the other hand, salts have a strong effect on the Nusselt number for high values of the buoyancy number and the
 617 temperature is increased by a factor between 1.5 and 2. As already stated, the formation of a stable, highly-salted layer
 618 at the bottom of the HP ice layer for high values of the buoyancy number leads to stratification of convection, which
 619 is less efficient at transporting heat. Therefore, it leads to a significant increase of the bottom temperature (Fig. 15.b),
 620 meaning more melt at the interface between the core and the HP ice.

621 The percentage of salts entering from the core that reach the ocean can be computed from the flow ratio f^o , which
 622 is the ratio of the total flux of salts across the upper boundary F_{salts}^o , which includes salts flowing into the ocean by
 623 melting of the topography at the interface and salts accreted to the ice by freezing of a small portion of the ocean, to
 624 the actual flux of salts coming from the core $F_{salts}^{eff} \sim 1$ computed by eq. 27:

$$f^o = \frac{F_{salts}^o (r^+)^2}{F_{salts}^{eff} (r^-)^2}. \quad (30)$$

625 This parameter is plotted on Fig. 16 as function of the buoyancy number for various values of the partition coefficient.
 626 As can be seen comparing Fig. 16.a and Fig. 16.b the flow ratio of salts f^o at the interface between the ice and the
 627 ocean is higher for a radius ratio $\gamma = 0.9$. The same can be observed for the bottom temperature and the top radial
 628 velocity, which are higher in that case (according to the scaling laws coefficients available in Table. 3). On Fig. 16.a
 629 we can observe that the flux of salts through the top interface is independent of B_{salts} for small values of B_{salts} but
 630 decreases with the buoyancy number for values larger than around 1. It is consistent with the fact that even if the radial
 631 velocity is relatively stable, the quantity of salts transported through the HP ice layer decreases with an increase of the
 632 buoyancy number. f^o also decreases with increasing values of the partition coefficient, because the greater the quantity
 633 of salts trapped in the ice during freezing at the top boundary, the lower the net flux of salts towards the ocean. Finally,
 634 Figure 16 shows that for $B_{salts} \geq 1$, f^o is roughly inversely proportional to B_{salts} , $f^o = c_F B_{salts}^{-1}$, which can easily
 635 be explained. Indeed, for $B_{salts} \geq 1$, the amount of salts transported by convection in the upper layer decreases for
 636 increasing values of the buoyancy number. In those cases, the effective buoyancy number in the upper convective layer
 637 is proportional to $\Delta C^i B_{salts}$, with ΔC^i the concentration of salts effectively realised in the upper layer, and should be
 638 less than or nearly equal to 1 for the salts to be easily transported by convection in the upper convective layer. It means
 639 that ΔC^i scales as $1/B_{salts}$. Also, as the convection in the upper layer is efficient ($B_{eff} \leq 1$), the flux of salts F_{salts}^o

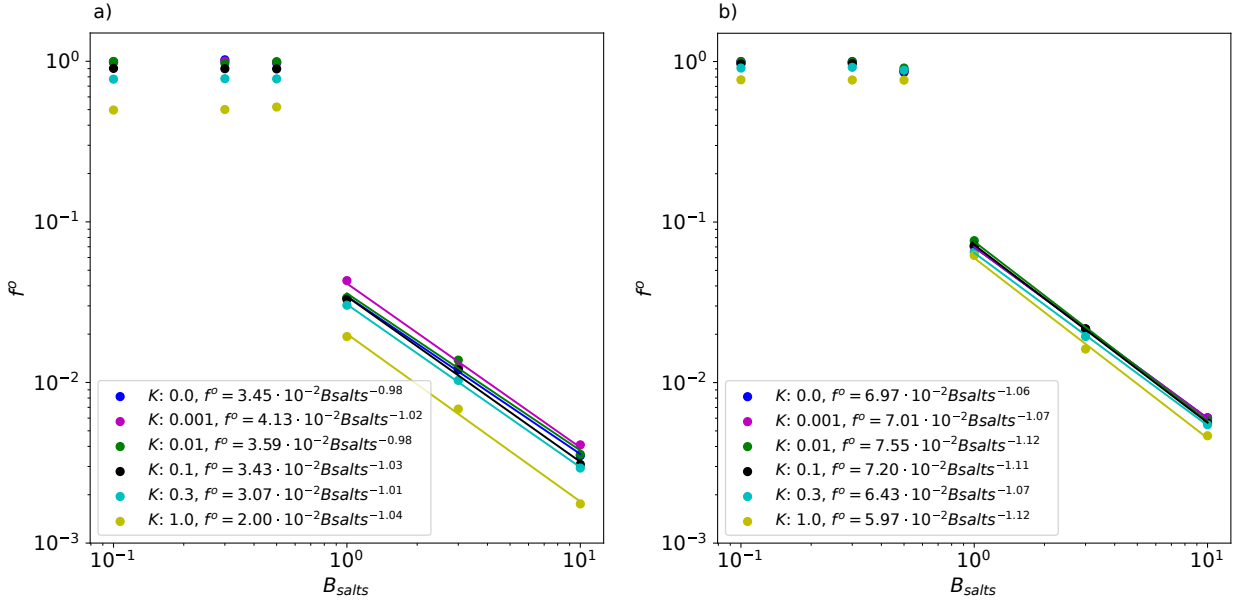


Figure 16: Flow ratio of salts through the ocean/ice interface f^o as function of the buoyancy number B_{salts} for various values of K and a Rayleigh number $Ra_q = 10^8$. a) is for a radius ratio $\gamma = 0.8$ and b) for $\gamma = 0.9$. Both panels display the relation $f^o = c_F B_{salts}^{p_F}$ (straight lines) for high values of the buoyancy number with c_F, p_F the scaling coefficients.

640 across the ice/ocean interface is the same as the flux of salts entering the upper layer from the lower one and should
 641 be $F_{salts}^o \sim \Delta C^i w_{top}$. Therefore, for a fixed radial velocity at the top, F_{salts}^o scales as $1/B_{salts}$. From eq. 30, for a fixed
 642 value of the flux of salts F_{salts}^{eff} entering the ice from the core, f^o also scales as $1/B_{salts}$.

643 As shown on Fig. 16, for high values of the buoyancy number, the fraction of salts from the core that ends up in the
 644 ocean is on the order of 0.1 to a few percent, depending on the buoyancy number and the partition coefficient, while it
 645 is around 50% for low values of the buoyancy number and a partition coefficient of 1 and in the range 75 – 100% for
 646 low values of the buoyancy number and lower partition coefficients.

647 3.4. Applications to Ganymede

648 The results discussed in the previous section for $K = 10^{-2}$ can be applied to specific planetary bodies. We use
 649 Ganymede as an example because its thick layer of HP ices could be considered an unfavourable environment for salts
 650 transfer, thus making it particularly interesting to estimate the efficiency of salt transfer from the core to the ocean.
 651 With a core radius of about 1 800 km and a total radius of 2 634 km (Hussmann et al., 2015), Ganymede is composed
 652 of a thick hydrosphere of about 834 km (See Table 4 for more details). The thickness of the HP ice layer is written as
 653 function of the core radius and the radius ratio γ as:

$$d = R^- \left(\frac{1-\gamma}{\gamma} \right). \quad (31)$$

654 For the radius ratios considered in Table 1, this gives a HP ice thickness between 200 and 450 km, which is in the
 655 actual range considered for Ganymede (Bland et al., 2009). As the radius ratio $\gamma = 0.8$ is the least favourable one in
 656 terms of radial velocity at the top, bottom temperature and effective flux of salts towards the ocean, all the following
 657 calculations are made for this case. First of all, the Rayleigh number can be computed for values in Table 4, with a
 658 viscosity of ice VI $\eta = 10^{15}$ Pa s and a heat flux from the core $q = 20$ mW m $^{-2}$ as reference values (Kalousová et al.,
 659 2018):

$$Ra_q = \frac{\alpha g q \rho d^4}{k \kappa \eta} = 4 \times 10^{11} \left(\frac{q}{20 \text{ mW m}^{-2}} \right) \left(\frac{d}{450 \text{ km}} \right)^4 \left(\frac{\eta}{10^{15} \text{ Pa s}} \right)^{-1}, \quad (32)$$

Table 4

Numerical application table for Ganymede. Most values (if not indicated otherwise) are from [Kalousová et al. \(2018\)](#).
^a [Husmann et al. \(2015\)](#).

^b [Grasset et al. \(2013\)](#); [Sotin and Tobie \(2004\)](#).

^c Computed from R^- for $\gamma = 0.8$ (max thickness) and $\gamma = 0.9$ (min thickness).

Parameter	Symbol	Ganymede	Unit
Thermal expansivity	α	1.5×10^{-4}	K^{-1}
Gravity	g	1.6	m s^{-2}
Thermal conductivity	k	1.6	$\text{Wm}^{-1}\text{K}^{-1}$
Thermal diffusivity	κ	4.3×10^{-7}	m^2s^{-1}
Reference density	ρ	1390	kgm^{-3}
HP ice viscosity	η	$10^{15} - 10^{17}$	Pa s
Heat flux for silicate core	q	10 – 40	mWm^{-2}
Radius	R	2 634 ^a	km
Core radius	R^-	1 800 ^a	km
Ocean radius	R_o	734 – 784	km
Hydrosphere thickness	d_h	834	km
Crust lh thickness	d_{lh}	50 – 100 ^b	km
HP ice thickness	d	200 – 450 ^c	km
Bottom melting temperature	T_m^-	332	K

660 which puts the HP ice layer of Ganymede in the large Rayleigh number regime of convection for any reasonable choice
 661 of parameter values.

662 We can use the scaling laws obtained earlier (fig. 15) to compute the radial velocity at the top and the bottom
 663 temperature for $\gamma = 0.8$ and various values of the buoyancy number, using the same reference values as for the Rayleigh
 664 number computed in eq. 32. Here we start with $B_{salts} = 1$:

$$w_{top} = 0.1 Ra_q^{0.52} \frac{\kappa}{d} = 3.3 \text{ m yr}^{-1} \left(\frac{q}{20 \text{ mW m}^{-2}} \right)^{0.52} \left(\frac{d}{450 \text{ km}} \right)^{1.08} \left(\frac{\eta}{10^{15} \text{ Pa s}} \right)^{-0.52}, \quad (33)$$

665

$$\frac{1}{\Delta \bar{T}} = 0.14 Ra_q^{0.25} \frac{k}{qd} = 1.98 \times 10^{-2} \text{ K}^{-1} \left(\frac{q}{20 \text{ mW m}^{-2}} \right)^{-0.75} \left(\frac{d}{450 \text{ km}} \right)^0 \left(\frac{\eta}{10^{15} \text{ Pa s}} \right)^{-0.25}. \quad (34)$$

666 Extrapolating the values from [Kalousová et al. \(2018\)](#) for a HP ice thickness of 450 km, the temperature T^+ at the
 667 interface between the ice and the ocean is equal to the melting temperature which is about 275 K. Therefore, still for
 668 $B_{salts} = 1$, the dimensional horizontal average bottom temperature \bar{T}^- for the reference values of all parameters is:

$$\bar{T}^- = \Delta \bar{T} + T^+ = 326 \text{ K} \quad (35)$$

669 The bottom temperature is on average very close to the melting temperature for pure water ice, $T_m^- = 332 \text{ K}$, which
 670 would imply the existence of at least pockets of melt at the interface with the core, especially as the presence of salts
 671 decreases the melting temperature. The actual value $T_m^- = 332 \text{ K}$ comes from [Kalousová et al. \(2018\)](#) and has been
 672 computed for pure water ice. In the present case ($B_{salts} = 1$ and $Ra_q = 1 \times 10^8$), the salts accumulate at the bottom of
 673 the ice layer, lowering the melting temperature and thus increasing the melting capacity at the interface. As previously
 674 stated, for a buoyancy number $B_{salts} = 1$, the accumulation of salts at the interface between the core and the ice
 675 leads to a stable, highly-salted layer at the bottom of the HP ice layer and to the stratification of convection. Stratified
 676 convection being less efficient in transporting heat, leads to the increase of the bottom temperature. Both these effects
 677 on temperature and melting temperature eventually lead to the total melting of this highly-salted layer.

678 We have also performed these calculations for $\gamma = 0.9$ from the data available in Table 3 and for $B_{salts} = 0$ and
 679 $B_{salts} = 1$ in order to compare the effect of low and high values of the buoyancy number on the radial velocity at top

Table 5

Results of the numerical application for Ganymede from values of Table 4 for rescaling and for $K = 10^{-2}$. Results for $\gamma = 0.8$ are computed from scaling laws available in Fig. 15 and in Table 3. Results for $\gamma = 0.9$ are computed from scaling laws available in Table 3. Values for T^+ come from Kalousová et al. (2018) for $d = 200$ km and extrapolated for $d = 450$ km.

γ	d (km)	Ra_q	B_{salts}	w_{top} (m yr ⁻¹)	$1/\Delta\bar{T}$ (K ⁻¹)	\bar{T}^- (K)	T^+ (K)
0.8	450	4×10^{11}	0	3.2	2.7×10^{-2}	312	275
			1	3.3	1.98×10^{-2}	326	275
0.9	200	1.6×10^{10}	0	1.5	2.6×10^{-2}	347	309
			1	1.1	1.5×10^{-2}	374	309

and the bottom temperature. All the results are displayed in Table 5. For $B_{salts} = 0$, the salts have no effect on the ice density and are transported passively through the HP ice layer. Therefore, the salts do not affect the dynamics and we fall back on the pure ice study case (Lebec et al., 2023). On the other hand, for a high buoyancy number $B_{salts} = 1$ the top radial velocity is of the same order of magnitude as for $B_{salts} = 0$, and the bottom temperature is higher. In addition, the accumulation of salts decreases the melting temperature, which means that the higher the amount of salts, the higher the melting capacity. For $\gamma = 0.9$, the bottom temperature is much higher, but the Nusselt number is close to the one obtained for the corresponding runs with $\gamma = 0.8$ due to the thinner HP ice shell. The bottom temperature is also much higher than the corresponding melting temperature $T_m^- = 332$ K for pure water ice and we expect substantial melting to occur in that case. The top radial velocity is on average two to three times smaller for $\gamma = 0.9$, compared to $\gamma = 0.8$, for a Rayleigh number 25 times smaller, also a consequence of the thinner HP ice layer.

The effective dimensional flux of salts F from the core per unit surface area can be estimated for values of the buoyancy number from 0 to 10, using eq. 9 and values from Table 4. Considering the reference value of the heat flux $q = 20$ mW m⁻², it gives us a range $F = 0 - 2.5 \times 10^{-4}$ m yr⁻¹. This can be used in accordance with Fig. 16 for $\gamma = 0.8$ to estimate a first range of the amount of salts transported across the ocean boundary per unit time. For high values of the buoyancy number, the fraction of the salts entering from the core that reach the ocean is on average (depending on the value of K) 0.3% for $B_{salts} = 10$ and 3% for $B_{salts} = 1$. This means that for high values of the buoyancy number the average flux of salts across the top boundary is around 7×10^{-7} m yr⁻¹. For a low buoyancy number such as $B_{salts} = 0.1$, the equivalent fraction is about 50 to nearly 100% depending on K , the flux of salts across the ice/ocean interface is of the order of 10^{-6} m yr⁻¹.

4. Discussion

In this study we considered a model with a uniform ice viscosity, while it should depend on pressure, temperature, salt concentration and on the fraction of liquid contained in the shell. We already performed a run with a varying viscosity in a previous study (Lebec et al., 2023) in order to check this point and the results for a model considering purely solid-state convection were quite close to those obtained with a constant viscosity. The difference here is the presence of salts, that would decrease the melting temperature of the ice. Also, the salts have a double effect on the efficiency of the convection, by allowing the salts/water mixture to remain liquid longer during the ascent through the bulk, but conversely to increase the ice density, which tends to impede the convection. Therefore, an improvement to this model would be to consider a two-phase model of convection in the HP ice layer to study all of these aspects.

Another limitation of this model that has already been pointed out in § 3.2.4 comes from the way the salts are added to the HP ice layer (See § 2.2.2) which affects the results of the runs. Indeed, for low values of the buoyancy number, the maximum concentration of salts in the shell is around the height at which the salts are added (Fig. 11.a). Also, for high values of the buoyancy number, a layering of the convection happens and the two independent convective layers separate at around this height (Fig. 13). As shown in Fig. 1.b and explained in the introduction, if a thin layer or isolated pockets of melt below the H₂O ice layer interact with the core and if this salted water is less dense than pure HP ices, it should rise through the HP ice layer. Its temperature would start to decrease until it partially, or totally, refreezes along its path (see Fig. 1.b). As we consider only convection in the solid state, this new salts/ice mixture is the focus of our study. Therefore, the salts we are studying are integrated into the ice at a given height above the bottom boundary, certainly close to the bottom interface, but not directly in contact with the core. This makes our model consistent, even if the height at which the salts are added to the ice is chosen arbitrarily and should not be interpreted quantitatively, as this height would undoubtedly depend on the type of salt and the implied solidus.

As stated in § 2.1.1, we impose a fixed flux of salts from the core, therefore assuming an infinite and continuous supply of salts. The amount of salts available is limited and should depend on the quantity of chemical elements capable of forming salts initially present in the core after differentiation of the planetary body and on their transport toward the core surface. A more realistic treatment would require to couple our model to a model for the dynamics and evolution of the core, which clearly falls beyond the scope of the present paper.

The present study shows that the presence of salts and their negative buoyancy makes the bottom temperature higher. Combined with their effect as a fusing agent in water (which is not modeled here) increases the chances of melting at the bottom of the HP ice layer compared to pure ice cases. In the case of a large buoyancy number, which leads to progressive enrichment in salts in a lower sublayer, when a certain quantity of salts accumulation at the bottom is reached, increasing the temperature at the interface with the core and decreasing the melting temperature, a thin secondary ocean between the HP ice layer and the core may appear. This ocean is likely to be very salty and it could be interesting to study its stability and its effect on the overall dynamics and on heat and mass transfer efficiency through the HP ice layer. In practice, it is difficult to constrain B_{salts} , which is why we chose a wide range of values to cover all possible dynamical regimes.

5. Conclusions

With this work, we investigate the effect of salts on the dynamics of a high-pressure ice shell between a solid core and a liquid ocean and on the efficiency of the transfer of salts between these two layers. Salts affect the dynamics through their effect on the density of the ice/salts mixture, the increase of which relative to the decrease of density due to temperature is quantified by the buoyancy number, B_{salts} . We model an influx of salts from the core, with a fixed heat flux at the bottom boundary, and we consider a mechanical phase change boundary condition at the top interface between the ice and the ocean, the effects of which on the dynamics and on the heat and mass transfer through a HP ice layer have already been studied previously (Lebec et al., 2023). For the sake of simplicity and to understand the effect of salts only, we chose to consider a uniform viscosity in the HP ice layer and convection in the solid state. Partial melting has already been considered in several studies (Kalousová and Sotin, 2018; Kalousová et al., 2018; Kalousová and Sotin, 2020) but with only pure ice. All of these effects could be interesting to combine in a future and more exhaustive study.

This paper sheds light on some of the questions that had been raised in our previous paper (Lebec et al., 2023). First of all, as already studied by Bolrão et al. (2021) in the context of magma oceans, if the ocean starts already salted and without an influx of salts from outside of the system, it ends up reaching a steady-state. For what can be considered to be low values of the effective buoyancy number, depending on the partition coefficient K of salts between the HP ice and the ocean at the top interface (see eq. 8), the system even reaches a chemical equilibrium.

Modeling an influx of salts from the core by adding a corresponding concentration of salts slightly above the interface between the core and the ice, corresponding to what would happen if the salts-enriched water at the bottom boundary rose through the bulk before recrystallizing at a certain height, two very distinct regimes can be observed. For low values of the buoyancy number, the salts are easily entrained by solid convection and all the salts entering the ice from the core reach the ocean. In contrast, for high values of the buoyancy number, the salts accumulate at the bottom of the HP ice layer and a layering of the convection happens at a depth corresponding to that at which the salts are added to the shell. This height corresponds to the crystallization point of the water/salt mixture, which depends on the salts properties. Also, for high values of the buoyancy number, the salts that accumulate at the bottom of the HP ice layer should increase the temperature of the salts/ice mixture and decrease the melting temperature, causing the formation of a thin secondary salty ocean between the HP ice layer and the core. Studying the effect of this secondary ocean on the HP ice layer dynamics could be an interesting topic for a future study.

Interestingly, the radial velocity at the ocean interface scales as a power 1/2 of the Rayleigh number, as for convection in pure ice (Lebec et al., 2023) and is only slightly affected by the concentration in salts of the HP ice layer. The Nusselt number scales as a power 1/5 of the Rayleigh number and the bottom temperature increases with the buoyancy numbers. We also obtained a scaling of the ratio of the salts flux across the ocean interface to that from the core as function of the buoyancy number and the exponent obtained is -1 . These dimensionless scaling laws can be applied to any planetary body with an internal structure corresponding to our model. This has been done for the case of Ganymede in § 3.4, choosing values in a relevant range for the least well-constrained parameters, such as the thickness of the ice, its viscosity and the heat flux from the core. This gives a radial velocity at the ice/water upper boundary around 3 m yr^{-1} for a HP ice thickness $d = 200 \text{ km}$ and 1.3 m yr^{-1} for a HP ice thickness $d = 450 \text{ km}$,

771 which would imply an efficient mass transfer through the interface and that salts reaching the interface should all go
 772 easily into the ocean. It is however difficult to provide a numerical value for the flux of salts reaching the ocean since it
 773 depends on the flux entering the ice from the core. A rough approximation for the large range of the buoyancy numbers
 774 considered in this study gave us a maximum flux around 10^{-6}m yr^{-1} .

775 Finally, if the temperature at the interface between the core and the ice reaches the melting temperature, all the salts
 776 that would enrich the ocean in the case of a small icy moon with a core in direct contact with a liquid ocean would end
 777 up in the ice in our case, provided the salty water is less dense than the HP ice. From here, two scenarios are possible.
 778 If the flux of salts from the core is low, in the sense that the buoyancy number is small and the density is only slightly
 779 larger than that of pure water ice, the transport of salts through the HP ice layer is efficient and all the salts coming from
 780 the core reach the ocean. On the other hand, if the flux of salts is large, convection is impeded in the lower part of the
 781 ice layer but is still possible in the upper part. We have shown that this process transports a fraction of the incoming
 782 flux such that the effective buoyancy number for the upper convecting layer is of order 0.5. In that case, only a small
 783 fraction of the salts coming from the core would reach the ocean, but considering a stronger flux of salts entering the
 784 ice, this small fraction could amount to a comparable flux reaching the ocean than in the case of a low flux from the
 785 core. To conclude about this aspect would require a better knowledge of the salts available in these moons. Therefore,
 786 future studies and space missions will be needed to better constrain the internal structure and composition of these
 787 water-rich bodies in order to conclude on their habitability.

788 6. Acknowledgments

789 We would like to thank the two anonymous reviewers for their constructive comments. Discussions with Anne
 790 Davaille, Gabriel Tobie, Christophe Sotin and Gaël Choblet helped us to improve the presentation of our results in
 791 this paper. Technical developments that enabled these simulations were made with support from the Swiss National
 792 Science Foundation (SNSF; grant nos. 200021E-164337 and ANR-15-CE31-0018-01). AM acknowledges the support
 793 of ERC through grant No. 787361-COBOM. We gratefully acknowledge support from the PSMN (Pôle Scientifique
 794 de Modélisation Numérique) of the ENS de Lyon for the computing resources.

795 Appendix 1. Numerical accuracy

796 As explained in § 3.2.2, we want to check the numerical accuracy of the imposed flux of salts by computing
 797 the effective flux of salts F_{salts}^{eff} from eq. 27. Figure 17 depicts F_{salts}^{eff} as function of the buoyancy number after the
 798 stabilization of the increase rate of the ocean concentration with time (see § 3.2.1 for more details). The two panels
 799 show F_{salts}^{eff} for various values of the buoyancy number and partition coefficients and contain the worst case among all
 800 runs of Table 1 in terms of error flux for $\gamma = 0.8$ (fig. 17a), which is for $B_{salts} = 3$ and $K = 10^{-1}$ and for $\gamma = 0.9$
 801 (fig. 17b), which is for $B_{salts} = 10$ and $K = 0$. The maximum error, all cases combined, is about 1.6%. This error is
 802 mostly due to the resolution at the bottom boundary. In the case of a large buoyancy number, the salts pile up at the
 803 bottom of the HP ice layer over time, which explains why the resolution must increase with B_{salts} . The worst case for
 804 both values of the radius ratio in terms of error flux is for a Rayleigh number of 10^9 and the resolution must be finer
 805 for higher Rayleigh numbers. Here we chose to refine the grid at the bottom boundary in order to limit this problem,
 806 as explained in § 2.2.1. We could further refine this boundary layer and increase the resolution of the simulations but
 807 increasing the resolution requires more numerical resources for an already very small error.

808 References

- 809 Agrusta, R., Morison, A., Labrosse, S., Deguen, R., Alboussière, T., Tackley, P.J., Dubuffet, F., 2020. Mantle convection interacting with magma
 810 oceans. *Geophys. J. Int.* 220, 1878–1892. doi:10.1093/gji/ggz549.
- 811 Baland, R.M., Tobie, G., Lefèvre, A., Van Hoolst, T., 2014. Titan's internal structure inferred from its gravity field, shape, and rotation state. *Icarus*
 812 237, 29–41. doi:10.1016/j.icarus.2014.04.007.
- 813 Bland, M.T., Showman, A.P., Tobie, G., 2009. The orbital–thermal evolution and global expansion of Ganymede. *Icarus* 200, 207–221.
 814 doi:10.1016/j.icarus.2008.11.016.
- 815 Bolrão, D.P., Ballmer, M.D., Morison, A., Rozel, A.B., Sanan, P., Labrosse, S., Tackley, P.J., 2021. Timescales of chemical equilibrium between
 816 the convecting solid mantle and over- and underlying magma oceans. *Solid Earth* 12, 421–437. doi:10.5194/se-12-421-2021.
- 817 Bouffard, M., Labrosse, S., Choblet, G., Fournier, A., Aubert, J., Tackley, P.J., 2017. A particle-in-cell method for studying double-diffusive
 818 convection in the liquid layers of planetary interiors. *J. Comput. Phys.* 346, 552–571. doi:10.1016/j.jcp.2017.06.028.

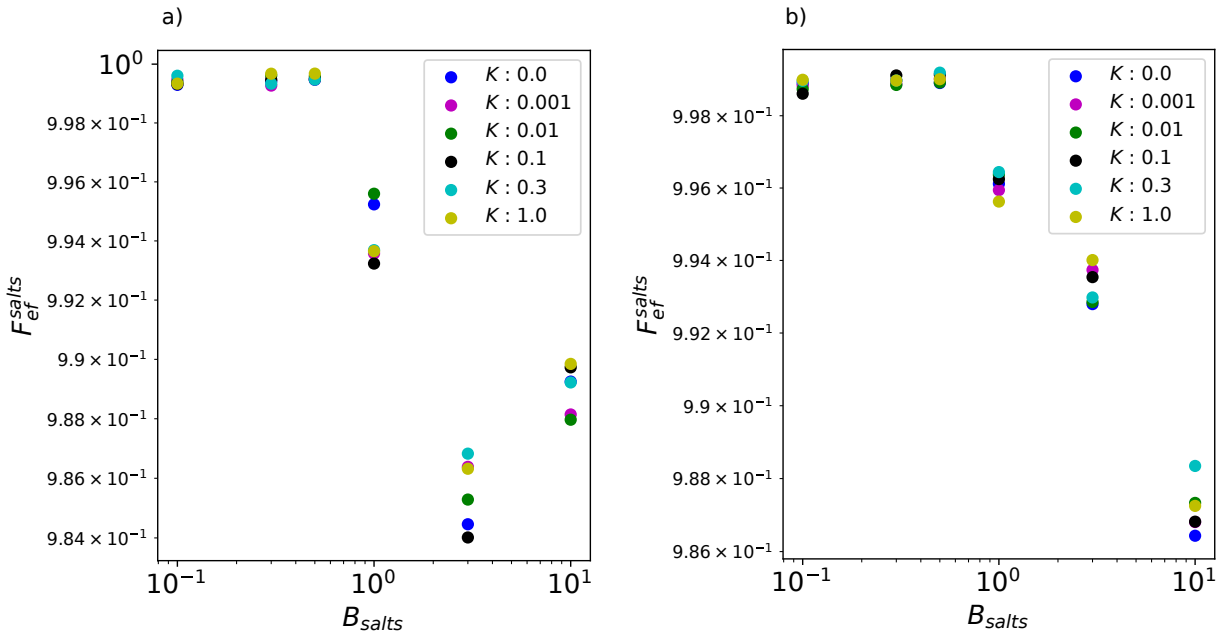


Figure 17: Flux of salts from the core as function of the buoyancy number for $Ra_q = 10^9$ and a) $\gamma = 0.8$ and b) $\gamma = 0.9$ for various values of the partition coefficient of the salts between the ocean and the HP ices at the top interface. This flux should be equal to 1 for all these simulations, these two figures contain the most extreme cases in terms of flux error for each radius ratio. The residual error is discussed in the text.

- 819 Béghin, C., Randriamboarison, O., Hamelin, M., Karkoschka, E., Sotin, C., Whitten, R.C., Berthelier, J.J., Grad, R., Simões, F., 2012. Analytic
 820 theory of Titan's Schumann resonance: Constraints on ionospheric conductivity and buried water ocean. *Icarus* 218, 1028–1042. doi:10.1016/
 821 j.icarus.2012.02.005.
- 822 Choblet, G., Tobie, G., Sotin, C., Kalousová, K., Grasset, O., 2017. Heat transport in the high-pressure ice mantle of large icy moons. *Icarus* 285,
 823 252–262. doi:10.1016/j.icarus.2016.12.002.
- 824 Deguen, R., 2013. Thermal convection in a spherical shell with melting/freezing at either or both of its boundaries. *J. Earth Sci.* 24, 669–682.
 825 doi:10.1007/s12583-013-0364-8.
- 826 Deguen, R., Alboussière, T., Cardin, P., 2013. Thermal convection in Earth's inner core with phase change at its boundary. *Geophys. J. Int.* 194,
 827 1310–1334. doi:10.1093/gji/ggt202.
- 828 Grasset, O., Dougherty, M., Coustenis, A., Bunce, E., Erd, C., Titov, D., Blanc, M., Coates, A., Drossart, P., Fletcher, L., Hussmann, H., Jaumann,
 829 R., Krupp, N., Lebreton, J.P., Prieto-Ballesteros, O., Tortora, P., Tosi, F., Van Hoolst, T., 2013. JUPITER ICY moons Explorer (JUICE): An ESA
 830 mission to orbit Ganymede and to characterise the Jupiter system. *Planet. Spa. Sci.* 78, 1–21. doi:10.1016/j.pss.2012.12.002.
- 831 Hernandez, J.A., Caracas, R., Labrosse, S., 2022. Stability of high-temperature salty ice suggests electrolyte permeability in water-rich exoplanet
 832 icy mantles. *Nature Commun.* 13, 3303. doi:10.1038/s41467-022-30796-5.
- 833 Hernlund, J.W., Tackley, P.J., 2008. Modeling mantle convection in the spherical annulus. *Phys. Earth Planet. Inter.* 171, 48–54. doi:10.1016/j.
 834 pepi.2008.07.037.
- 835 Hussmann, H., Sotin, C., Lunine, J.I., 2015. 10.18 - Interiors and Evolution of Icy Satellites. *Treatise on Geophys.* 10, 605–635. doi:10.1016/
 836 B978-0-444-53802-4.00178-0.
- 837 Iess, L., Jacobson, R.A., Ducci, M., Stevenson, D.J., Lunine, J.I., Armstrong, J.W., Asmar, S.W., Racioppa, P., Rappaport, N.J., Tortora, P., 2012.
 838 The Tides of Titan. *Science* 337, 457–459. doi:10.1126/science.1219631.
- 839 Iess, L., Rappaport, N.J., Jacobson, R.A., Racioppa, P., Stevenson, D.J., Tortora, P., Armstrong, J.W., Asmar, S.W., 2010. Gravity Field, Shape, and
 840 Moment of Inertia of Titan. *Science* 327, 1367–1369. doi:10.1126/science.1182583.
- 841 Journaux, B., Daniel, I., Caracas, R., Montagnac, G., Cardon, H., 2013. Influence of NaCl on ice VI and ice VII melting curves up to 6GPa,
 842 implications for large icy moons. *Icarus* 226, 355–363. doi:10.1016/j.icarus.2013.05.039.
- 843 Journaux, B., Daniel, I., Petitgirard, S., Cardon, H., Perrillat, J.P., Caracas, R., Mezouar, M., 2017. Salt partitioning between water and high-
 844 pressure ices. implication for the dynamics and habitability of icy moons and water-rich planetary bodies. *Earth Planet. Sci. Lett.* 463, 36–47.
 845 doi:10.1016/j.epsl.2017.01.017.
- 846 Kalousová, K., Sotin, C., 2018. Melting in High-Pressure Ice Layers of Large Ocean Worlds—Implications for Volatiles Transport. *Geophys. Res.*
 847 *Lett.* 45, 8096–8103. doi:10.1029/2018GL078889.

- 848 Kalousová, K., Sotin, C., 2020. Dynamics of Titan's high-pressure ice layer. *Earth Planet. Sci. Lett.* 545, 116416–116416. doi:[10.1016/j.epsl.2020.116416](https://doi.org/10.1016/j.epsl.2020.116416). publisher: Elsevier B.V.
- 849 Kalousová, K., Sotin, C., Choblet, G., Tobie, G., Grasset, O., 2018. Two-phase convection in Ganymede's high-pressure ice layer — Implications
850 for its geological evolution. *Icarus* 299, 133–147. doi:[10.1016/j.icarus.2017.07.018](https://doi.org/10.1016/j.icarus.2017.07.018).
- 851 Kivelson, M., Khurana, K., Volwerk, M., 2002. The Permanent and Inductive Magnetic Moments of Ganymede. *Icarus* 157, 507–522.
852 doi:[10.1006/icar.2002.6834](https://doi.org/10.1006/icar.2002.6834).
- 853 Labrosse, S., Morison, A., Deguen, R., Alboussière, T., 2018. Rayleigh–Bénard convection in a creeping solid with melting and freezing at either
854 or both its horizontal boundaries. *J. Fluid Mech.* 846, 5–36. doi:[10.1017/jfm.2018.258](https://doi.org/10.1017/jfm.2018.258).
- 855 Le Bars, M., Davaille, A., 2004. Large interface deformation in two-layer thermal convection of miscible viscous fluids. *J. Fluid Mech.* 499, 75–110.
856 doi:[10.1017/S0022112003006931](https://doi.org/10.1017/S0022112003006931).
- 857 Lebec, L., Labrosse, S., Morison, A., Tackley, P.J., 2023. Scaling of convection in high-pressure ice layers of large icy moons and implications for
858 habitability. *Icarus* 396, 115494. doi:[10.1016/j.icarus.2023.115494](https://doi.org/10.1016/j.icarus.2023.115494).
- 859 Leliwa-Kopystyński, J., Maruyama, M., Nakajima, T., 2002. The Water–Ammonia Phase Diagram up to 300 MPa: Application to Icy Satellites.
860 *Icarus* 159, 518–528. doi:[10.1006/icar.2002.6932](https://doi.org/10.1006/icar.2002.6932).
- 861 Mitri, G., Meriggiola, R., Hayes, A., Lefevre, A., Tobie, G., Genova, A., Lunine, J.I., Zebker, H., 2014. Shape, topography, gravity anomalies and
862 tidal deformation of Titan. *Icarus* 236, 169–177. doi:[10.1016/j.icarus.2014.03.018](https://doi.org/10.1016/j.icarus.2014.03.018).
- 863 Soderlund, K.M., Kalousová, K., Buffo, J.J., Glein, C.R., Goodman, J.C., Mitri, G., Patterson, G.W., Postberg, F., Rovira-Navarro, M., Rückriemen,
864 T., Saur, J., Schmidt, B.E., Sotin, C., Spohn, T., Tobie, G., Van Hoolst, T., Vance, S.D., Vermeersen, B., 2020. Ice-Ocean Exchange Processes
865 in the Jovian and Saturnian Satellites. *Space Sci. Rev.* 216, 80. doi:[10.1007/s11214-020-00706-6](https://doi.org/10.1007/s11214-020-00706-6).
- 866 Sotin, C., Kalousová, K., Tobie, G., 2021. Titan's Interior Structure and Dynamics After the Cassini-Huygens Mission. *Annual Review of Earth
867 and Planet. Sci.* 49, 579–607. doi:[10.1146/annurev-earth-072920-052847](https://doi.org/10.1146/annurev-earth-072920-052847).
- 868 Sotin, C., Tobie, G., 2004. Internal structure and dynamics of the large icy satellites. *Comptes Rendus Physique* 5, 769–780. doi:[10.1016/j.
869 crhy.2004.08.001](https://doi.org/10.1016/j.crhy.2004.08.001).
- 870 Tackley, P.J., 2008. Modelling compressible mantle convection with large viscosity contrasts in a three-dimensional spherical shell using the
871 yin-yang grid. *Phys. Earth Planet. Inter.* 171, 7–18. doi:[10.1016/j.pepi.2008.08.005](https://doi.org/10.1016/j.pepi.2008.08.005).
- 872 Tackley, P.J., King, S.D., 2003. Testing the tracer ratio method for modeling active compositional fields in mantle convection simulations. *Geochem.
873 Geophys. Geosyst.* 4. doi:[10.1029/2001GC000214](https://doi.org/10.1029/2001GC000214).
- 874 Zolotov, M.Y., Kargel, J.S., 2009. On the chemical composition of europa's icy shell, ocean, and underlying rocks. Tucson, AZ: University of
875 Arizona Press 431, 431 – 458. doi:[10.2307/j.ctt1xp3wdw](https://doi.org/10.2307/j.ctt1xp3wdw).
- 876